Theory Manual for the Steel Corrosion Model Version 1.0

NWMO TR-2009-07 March 2009

Fraser King[1] and Miroslav Kolar[2]

[1]Integrity Corrosion Consulting Ltd.
[2]LS Computing Ltd.

nwmo
NUCLEAR WASTE MANAGEMENT ORGANIZATION
SOCIÉTÉ DE GESTION DES DÉCHETS NUCLÉAIRES

Nuclear Waste Management Organization
22 St. Clair Avenue East, 6th Floor
Toronto, Ontario
M4T 2S3
Canada

Tel: 416-934-9814
Web: www.nwmo.ca

Theory Manual for the Steel Corrosion Model Version 1.0

NWMO TR-2009-07

March 2009

Fraser King[1] **and Miroslav Kolar**[2]
[1]Integrity Corrosion Consulting Ltd.
[2]LS Computing Ltd.

ABSTRACT

Title: **Theory Manual for the Steel Corrosion Model Version 1.0**
Report No.: **NWMO TR-2009-07**
Author(s): Fraser King[1] and Miroslav Kolar[2]
Company: [1]Integrity Corrosion Consulting Ltd. [2]LS Computing Ltd.
Date: March 2009

Abstract
A model for the prediction of the anaerobic corrosion behaviour of carbon steel used fuel containers in a deep geological repository in sedimentary host rock in Canada is described. The model is termed the Steel Corrosion Model Version 1.0 (SCM V1.0). The model is designed to predict not only the corrosion behaviour of the container but also the impacts of corrosion products, specifically dissolved ferrous species and hydrogen, on the other barriers in the system, particularly the bentonite or bentonite/sand buffer. This theory manual describes both the conceptual mechanistic model and the mathematical model used for predictions.

The conceptual model is based on a reaction scheme that includes a total of 13 species, namely: a dissolved ferrous-chloro complex $FeCl^+(aq)$, a dissolved ferrous-carbonate complex ion $Fe(CO_3)_2^{2-}(aq)$, dissolved ferrous-hydroxy ion $FeOH^+(aq)$, dissolved hydrogen $H_2(aq)$, the bicarbonate ion $HCO_3^-(aq)$, the chloride ion $Cl^-(aq)$, solid ferrous hydroxide $Fe(OH)_2(s)$, magnetite $Fe_3O_4(s)$, siderite or iron carbonate $FeCO_3(s)$, adsorbed ferrous species $Fe(II)_{ADS}$, iron-altered clay Fe(clay), calcite $CaCO_3(s)$, and hydrogen gas $H_2(g)$. These species participate in a number of interfacial electrochemical reactions, precipitation and dissolution processes, adsorption and desorption of cations on bentonite clay, mass transport towards and away from the container, alteration of the bentonite clay by reaction with Fe(II), gas generation and transport, and partitioning between aqueous and gaseous phases.

Other features of the model include a detailed analysis of corrosion product film formation processes, as part of which the time-dependent thickness and porosity of the film is predicted. The effects of repository saturation on mass transport and on the rates of interfacial and other processes are considered. Hydrogen generation and transport is also treated in the model, as is the alteration of clay by reaction with dissolved Fe(II) species.

The mathematical model is based on a series of 15 one-dimensional reaction-transport equations, one each for the 13 chemical species, one for the porosity of the corrosion product film, and one for temperature. These equations are solved subject to various boundary and initial conditions within a spatial grid designed to represent the geometry of the repository. The most important of these boundary conditions are the electrochemical expressions that describe the rates of the interfacial corrosion reactions. By using the reactions as boundary conditions for the solution of the mass-balance equations, the model is able to not only couple the corrosion behaviour of the container to the evolution of the repository environment, but also to predict the time dependence of the corrosion potential and corrosion rate through the use of mixed-potential theory.

The theory manual describes the conceptual model and reaction scheme in some detail, along with a discussion of the various underlying assumptions in the model. The mathematical model is also described, including the 15 reaction-transport equations, the initial and boundary conditions, the spatial grid, and the finite-difference technique used for the numerical solution.

TABLE OF CONTENTS

LIST OF TABLES

Page

LIST OF FIGURES

Page

1. INTRODUCTION

The Nuclear Waste Management Organization (NWMO) is carrying out a research and development (R&D) program to support implementation of Adaptive Phase Management for the long-term management of Canada's used nuclear fuel (NWMO 2005). The NWMO's R&D program includes technologies associated with a deep geological repository (DGR) for used fuel in a suitable geological formation, such as crystalline rock or sedimentary deposits. Any such repository would be based on a multi-barrier design, comprising a number of natural and engineered barriers (Russell and Simmons 2003). One of the engineered barriers would be a long-lived metallic used-fuel container (UFC) designed to provide long-term containment and isolation of used fuel for a considerable length of time.

Two materials are being considered as corrosion barriers for the UFC. Copper has long been considered in Canada, with oxygen-free, phosphorus-doped (OFP) copper as the reference container material for a DGR in crystalline rock (Gierszewski et al. 2004, Maak 1999). More recently, carbon steel (C-steel) has been considered as an alternative to copper for a repository in sedimentary deposits (King 2005a,b; 2007). A detailed repository design for a DGR in sedimentary rock in Canada is being studied. For the purposes of discussion, a repository design similar to that for Opalinus Clay in Switzerland is used here.

Carbon steel is a candidate container material in a number of national waste management programs considering a DGR in sedimentary host rock (Andra 2005, Nagra 2002). Historically, C-steel containers have been assumed to have shorter lifetimes than containers fabricated from copper.

The expected corrosion behaviour of a C-steel UFC in a Canadian repository in sedimentary rock has been discussed by King (2005a) and a conceptual corrosion model developed (King 2007). Most importantly, the corrosion behaviour of the container changes as the environment within the repository evolves. Three phases in the evolution of the repository environment have been defined; namely, an early unsaturated aerobic phase, a transition period at the end of which the repository environment will be anoxic, and a long-term anaerobic phase. Depending upon the rate of repository saturation, the transition and long-term anaerobic phases may involve both saturated and unsaturated conditions.

The corrosion model described in this report is focused on the corrosion behaviour during the long-term anaerobic phase. Therefore, no consideration is given to either the aerobic phase or the transitional period during which the oxidized corrosion products formed early in the repository evolution are reduced to ferrous species. The important corrosion processes during the anaerobic phase are: (i) the rate of uniform corrosion, (ii) the rate of hydrogen generation and transport, and (iii) the possibility of H-related degradation mechanisms. In the absence of environmentally assisted cracking (either due to hydrogen or via stress corrosion cracking), the most likely failure mechanism is uniform corrosion. Therefore, a reactive-transport model similar to that previously developed for copper UFC (King and Kolar 2000, 2006) is appropriate for the lifetime prediction of C-steel containers.

This theory manual describes the conceptual and mathematical bases of a corrosion model for C-steel UFC in an anaerobic deep geological repository. The model is referred to as the Steel Corrosion Model Version 1.0 (SCM V1.0). Although C-steel is primarily considered as a candidate container material for a DGR in sedimentary rock, the model itself is applicable to

other geological settings. The conceptual model described in Section 2 includes a detailed discussion of each of the processes included in the reaction scheme adopted for the SCM V1.0. In addition to processes that affect the corrosion behaviour of the container, the consequences of corrosion products on the integrity of other engineered barriers, specifically the effects of gaseous H_2 and dissolved Fe(II), are also considered. The mathematical basis for the SCM is analogous to that for the CCM series of models and comprises a set of 1-dimensional reactive-transport equations, that are solved using finite difference methods within a spatial grid using appropriate mathematical boundary conditions.

2. CONCEPTUAL MODEL

2.1 REACTION SCHEME

Figure 1 shows the reaction scheme for the SCM V1.0. The reaction scheme includes a series of interfacial electrochemical reactions coupled to various mass-transport, adsorption/ desorption, precipitation/dissolution, iron-clay interaction, and gas partitioning processes occurring in the near field. Because the interfacial processes are coupled to the near-field processes in the model, the effects of the evolution of the near-field environment on the corrosion behaviour of the UFC are directly accounted for in the SCM.

The thirteen species considered in the model include: a dissolved ferrous-chloro complex $FeCl^+(aq)$, a dissolved ferrous-carbonate complex ion $Fe(CO_3)_2^{2-}(aq)$, dissolved ferrous-hydroxy ion $FeOH^+(aq)$, dissolved hydrogen $H_2(aq)$, the bicarbonate ion $HCO_3^-(aq)$, the chloride ion $Cl^-(aq)$, solid ferrous hydroxide $Fe(OH)_2(s)$, magnetite $Fe_3O_4(s)$, siderite or iron carbonate $FeCO_3(s)$, adsorbed ferrous species $Fe(II)_{ADS}$, iron-altered clay Fe(clay), calcite $CaCO_3(s)$, and hydrogen gas $H_2(g)$.

Each of the processes considered in the model is discussed in more detail below.

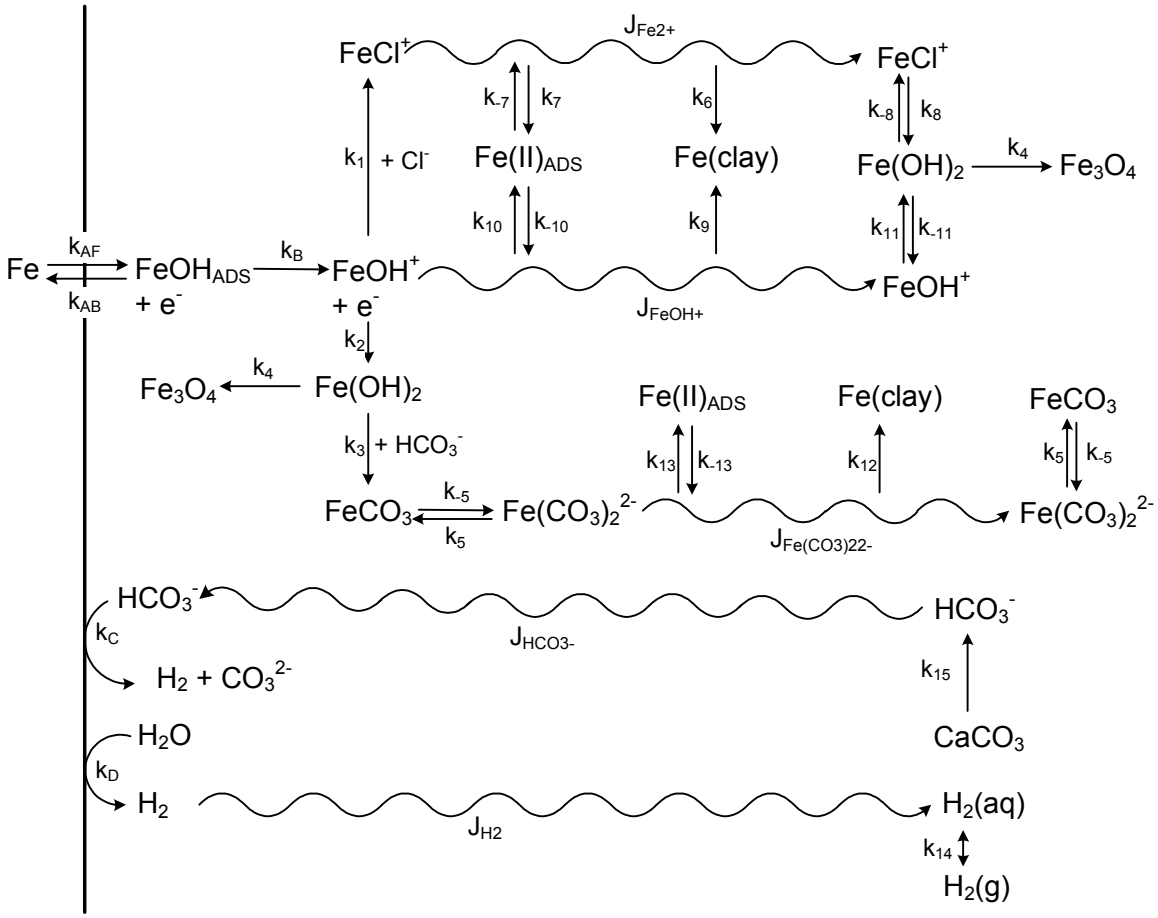

Figure 1: Reaction Scheme for the Steel Corrosion Model Version 1.0 (SCM V1.0).

2.2 PROCESSES CONSIDERED

2.2.1 Interfacial Electrochemical Reactions

2.2.1.1 Anodic Processes

The anodic dissolution of Fe in aqueous solution has been the subject of extensive study (Albani et al. 1990; Ashley and Burstein 1991; Bockris and Drazic 1962; Bockris and Reddy 1970; Bockris et al. 1961; Castro and Vilche 1991, 1992; Castro et al. 1991; Lee et al. 2006a,b; MacFarlane and Smedley 1986; Vela et al. 1986). Although a number of mechanisms have been proposed, it is generally agreed that the initial stages of oxidation proceed through an adsorbed $FeOH_{ADS}$ intermediate, followed by a second electron transfer to produce a surface Fe(II) species:

$$Fe + H_2O = FeOH_{ADS} + H^+ + e^- \quad (1a)$$

$$FeOH_{ADS} \rightarrow FeOH^+ + e^- \quad (1b)$$

The first electron transfer reaction is considered to be fast, with the second electron transfer step being rate controlling. These interfacial reactions are denoted by rate constants k_{AF}/k_{AB} and k_B, respectively, in Figure 1.

The interfacial $FeOH^+$ species can undergo a number of processes (Figure 1). Although its solubility is limited, $FeOH^+$ could diffuse away from the container surface into the bentonite or bentonite/sand buffer. More likely, however, $FeOH^+$ will precipitate as $Fe(OH)_2$, a species commonly observed during the initial dissolution of Fe (Castro and Vilche 1991, 1992; Castro et al. 1991; Odziemkowski et al. 1998; Simpson and Melendres 1996), according to

$$FeOH^+ + OH^- \rightarrow Fe(OH)_2(s) \quad (2)$$

denoted by rate constant k_2 in Figure 1.

In the presence of Cl^- ions there is competition between OH^- and Cl^- for surface adsorption sites and alternative species, such as $FeCl_{ADS}$ or Fe(OH)Cl, may be formed (Ashley and Burstein 1991, MacFarlane and Smedley 1986). The relative concentration of surface phases depends on the relative concentrations of Cl^- and OH^- (pH) ions. In Cl^--dominated solutions, therefore, $FeOH^+$ is more likely to transform into a ferrous-chloro species rather than precipitate as $Fe(OH)_2$. In the SCM V1.0, the competition between OH^- and Cl^- ions is assumed to result in the formation of $FeCl^+$ in chloride-dominated solutions:

$$FeOH^+ + Cl^- \rightarrow FeCl^+ + OH^- \quad (3)$$

where the overall kinetics are taken to be second order (first order with respect to the concentrations of $FeOH^+$ and Cl^-). At high $[Cl^-]$, the free Fe(II) ion could exist in a number of ferrous-chloride complexes, such as $FeCl^+$, $FeCl_2$, $FeCl_3^-$, etc., which are represented in the SCM V1.0 by the single species $FeCl^+$.

The formation of Fe(III) is not included in the SCM V1.0 since the potential under anaerobic conditions is more negative than that required for the formation of ferric species.

2.2.1.2 Cathodic Processes

The cathodic process under anaerobic conditions results in the formation of H_2 (Bockris and Reddy 1970, Turnbull and May 1987). Hydrogen evolution involves the cathodic reduction of the hydrogen source (see below) to produce adsorbed H atoms. For example, if H_2O is the source of hydrogen the reaction can be written as

$$H_2O + e^- \rightarrow H_{ADS} + OH^- \quad (4)$$

Following the electron-transfer process, H_2 is produced via one of two processes (Bockris and Reddy 1970); namely, the Volmer-Tafel pathway

$$2H_{ADS} \rightarrow H_2 \quad (5a)$$

or the Volmer-Heyrovsky pathway

$$H_{ADS} + H_2O + e^- \rightarrow H_2 + OH^- \quad (5b)$$

(Alternatively, the adsorbed H atoms can diffuse into the steel substrate, potentially resulting in various H-related degradation mechanisms).

Regardless of which pathway is followed, the overall hydrogen evolution reaction can be written as

$$H_2O + e^- \rightarrow \tfrac{1}{2} H_2 + OH^- \quad (6)$$

Turnbull and May (1987) report detailed electrochemical kinetic data for this reaction in NaCl solutions, which is denoted in Figure 1 by rate constant k_D.

Water is not the only potential source of hydrogen in the repository. At sufficiently low pH, the reduction of H^+ or H_3O^+ ions is a more-likely source of hydrogen than the reduction of H_2O. However, at the expected pH of buffer pore water (pH 7.5-8), the concentration of H^+ (of the order of 10^{-7}-10^{-8} mol·dm^{-3}) is significantly less than that of H_2O (55 mol·dm^{-3}).

Because of the presence of carbonate minerals in the bentonite clay, the pore water will contain bicarbonate ions (HCO_3^-) which could also act as a source of hydrogen

$$HCO_3^- + e^- \rightarrow \tfrac{1}{2} H_2 + CO_3^{2-} \quad (7)$$

represented by rate constant k_C in Figure 1.

(The reduction of carbonic acid (H_2CO_3) is not included in the reaction scheme because the concentration will be at least an order of magnitude less than that of HCO_3^- since the pK for the dissociation of H_2CO_3 is –6.5).

2.2.2 Film Formation

Because the solubility of Fe(II) is limited at the pH of buffer pore water (of the order of 10^{-5} mol·dm^{-3}, Pourbaix 1974), film formation is an important aspect of the corrosion behaviour of C-steel in near-neutral pH solutions.

Surface films could affect the corrosion behaviour of the UFC in a number of ways, including:

- restricting the mass transport of reactants to, and of corrosion products away from, the corroding surface,
- blocking the surface from further dissolution (if the film is non-conducting), and
- changing the anode and cathode surface areas and their ratio (if the film is sufficiently conducting that it can support electrochemical reactions).

Of these possible impacts, the surface blocking and restriction on mass transport to and from the surface are typically the most important. Both of these effects result in a decrease in corrosion rate with time, as observed experimentally (King 2008a, Smart et al. 2001). For some alloy systems the surface film forms a continuous passive layer on the surface, with rate control by solid-state diffusion across the film. In other cases, a porous but protective film is formed, generally comprising an out porous layer formed by a dissolution-precipitation process overlying an inner barrier layer.

The available experimental evidence suggests that the films formed on C-steel under repository conditions will be of the latter type (King 2008a). Both Fe_3O_4 and iron carbonate species have been reported, with magnetite more common in experiments in bulk solution and $FeCO_3$ being observed in the presence of compacted bentonite. Furthermore, although the observed corrosion rate decreases with time, there is evidence for the establishment of a steady-state constant corrosion rate at long times (King 2008a).

Various precipitated corrosion products are included in the model, with the precise nature of the film determined by the relative rates of precipitation. Ferrous hydroxide ($Fe(OH)_2$) is considered to be the most likely species to form initially, and is commonly observed experimentally during the initial stages of corrosion and oxidation of C-steel (Simpson and Melendres 1996, Odziemkowski et al. 1998)

$$FeOH^+ + OH^- \xrightarrow{k_2} Fe(OH)_2 \qquad (8)$$

the rate of which is assumed to be proportional to the concentration of $FeOH^+$.

Ferrous hydroxide is known to convert into Fe_3O_4 (the Schikorr reaction) (Odziemkowski et al. 1998)

$$3Fe(OH)_2 \xrightarrow{k_4} Fe_3O_4 + H_2 + 2H_2O \qquad (9)$$

The rate of the conversion of $Fe(OH)_2$ to Fe_3O_4 is taken to be proportional to the concentration of $Fe(OH)_2$.

In the presence of carbonate, $Fe(OH)_2$ can also be converted to ferrous carbonate $FeCO_3$

$$Fe(OH)_2 + HCO_3^- \xrightarrow{k_3} FeCO_3 + OH^- + H_2O \quad (10)$$

the rate of which is proportional to the concentrations of HCO_3^- and $Fe(OH)_2$.

In the SCM V1.0, the corrosion product film is treated as a porous deposit which serves to block the surface from further dissolution and to restrict mass transport of species to and from the surface. Although the existence of a thin barrier layer at the metal/film interface is acknowledged, this layer is not specifically modelled. The porous deposit thickens with time, with the layer growing by precipitation of the respective solid at the location at which super-saturation occurs (rather than, for instance, growth occurring only at the film/solution interface). To avoid the surface becoming completely blocked by precipitated solid, a minimum interfacial film porosity is imposed at the C-steel surface. The use of a minimum interfacial film porosity can be rationalized on the basis that local acidification within the pores of the film will tend to prevent precipitation and to maintain an open porosity.

2.2.3 Interaction Between Fe(II) and Bentonite

A primary consideration in the development of the design of the engineered barrier system is that no barrier should adversely affect the function of other barriers. One possible adverse effect is the interaction of Fe(II) produced by corrosion of a C-steel container with the bentonite clay in the buffer material. This interaction may take one of two forms; reversible adsorption/desorption of Fe(II) and the irreversible alteration of the clay by reaction with Fe(II).

2.2.3.1 Reversible Adsorption/desorption

Sorption of cations by bentonite involves an ion-exchange or surface complexation process. Adsorption and desorption processes are relatively fast and are often assumed to be in equilibrium. However, in some cases, for example the desorption of strongly sorbed species such as Cu(II) (Ryan and King 1994), the process may not be at equilibrium, even for the slow transit times through compacted bentonite or bentonite/sand buffer (King et al. 1996).

As in the CCM series of corrosion models (King and Kolar 2000), sorption is treated as a reversible process in the SCM V1.0 using a kinetically based Langmuir adsorption isotherm. Three adsorbates are considered in the model; $FeCl^+$, $FeOH^+$, and $Fe(CO_3)_2^{2-}$. The adsorption and desorption processes, and their respective rate constants, are given by

$$FeCl^+ \underset{k_{-7}}{\overset{k_7}{\rightleftharpoons}} Fe(II)_{ADS} + Cl^- \quad (11)$$

$$FeOH^+ \underset{k_{-10}}{\overset{k_{10}}{\rightleftharpoons}} Fe(II)_{ADS} + OH^- \quad (12)$$

and

$$Fe(CO_3)_2^{2-} \underset{k_{-13}}{\overset{k_{13}}{\rightleftharpoons}} Fe(II)_{ADS} + 2CO_3^{2-} \quad (13)$$

The rate of adsorption is considered to be second order overall; first order with respect to the concentration of adsorbate and first order with respect to the concentration of free exchange

sites on the bentonite. The rate of desorption of Fe(II) in the form of either $FeCl^+$ and $FeOH^+$ is assumed to first order overall and to be proportional to the concentration of $Fe(II)_{ADS}$. In the case of the desorption of Fe(II) as $Fe(CO_3)_2^{2-}$ ions, the rate of desorption is assumed to be second order overall; first order with respect to the concentration of $Fe(II)_{ADS}$ and first order with respect to the concentration of HCO_3^- (which will be the predominant carbonate species present in the pore water at the expected pH of pH 7.5-8).

2.2.3.2 Irreversible Clay Alteration

The possible alteration of smectite clays by interaction with Fe(II) has received increasing attention over the past few years (Carlson et al. 2006, Marcos 2003, Johnson et al. 2005, Perronnet et al. 2008, Savage et al. 2009, Wersin and Snellman 2008). The primary concern is that swelling smectite clays may be altered into non-swelling forms, with a consequent loss of swelling pressure, reduced sorption capacity, compromised sealing properties, and possible loss of the apparent restriction on microbial activity observed in highly compacted bentonite.

The currently available experimental evidence provides various observations of the consequences of Fe(II) interaction with bentonite. There appears to be two main pathways (Wersin and Snellman 2008): one involving the formation of Fe-rich smectite clays, such as saponite and nontronite; and a second pathway that results in the formation of non-swelling clay minerals, such as berthierine, constedtite, and chlorites. There is a lack of information on the kinetics or thermodynamics of smectite alteration and no clear understanding of whether smectite or non-swelling clays will result from Fe(II)-bentonite interactions under repository conditions. Another outstanding question is the possible reduction of structural Fe(III) in dioctohedral lattice positions by H_2 produced by corrosion.

Various attempts have been made to model the Fe(II)-bentonite interaction process, despite the lack of kinetic and thermodynamic data. Savage et al. (2009) have suggested a sequence of alteration phases with berthierine predominating for periods up to 10,000 years. Using a simple reactive-transport model, Johnson et al. (2005) suggested that it would take of the order of several hundred thousand years for the reaction front to extend 20-30 cm from the container, depending upon the nature of the predominant corrosion product (and, therefore, on the interfacial [Fe(II)]). The slow progression of the alteration front is primarily a consequence of the slow rate of diffusion in compacted buffer, an effect that is enhanced by the reduction in porosity that could accompany clay alteration or cementation (Wersin and Snellman 2008).

Given the current uncertainty in the mechanism and rate of bentonite alteration by Fe(II), the process is treated simply here as an irreversible first-order reaction, with the rate proportional to the concentration of the respective Fe(II) species (i.e., $FeCl^+$, $FeOH^+$, and $Fe(CO_3)_2^{2-}$). The alteration product is denoted as Fe(clay). The corresponding reactions are (Figure 1)

$$FeCl^+ \xrightarrow{k_6} Fe(clay) + Cl^- \quad (14)$$

$$FeOH^+ \xrightarrow{k_9} Fe(clay) + OH^- \quad (15)$$

and

$$Fe(CO_3)_2^{2-} \xrightarrow{k_{12}} Fe(clay) + 2HCO_3^- + 2OH^- \quad (16)$$

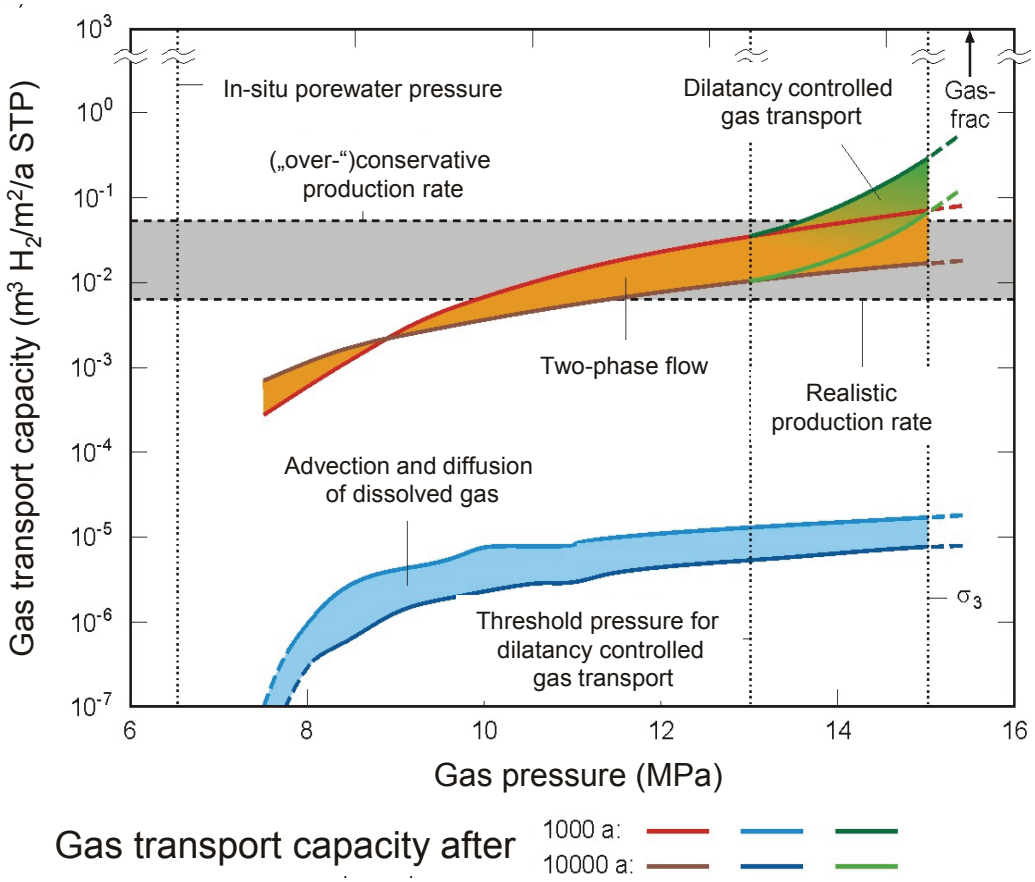

Figure 2: Gas Transport Capacity for Various Gas Transport Mechanisms in Opalinus Clay as a Function of the Total Pressure (Nagra 2004).

2.2.4 Hydrogen Generation and Transport

Hydrogen is generated by the interfacial reduction of H_2O (Reaction (6)) or HCO_3^- (Reaction (7)). The majority of this hydrogen is not absorbed by the steel but is released from the surface as H_2. The solubility of H_2 in water is limited and it is inevitable that a H_2 gas phase will form in the repository.

Nagra (2004) have established the capacity of Opalinus Clay to transport gas via various mechanisms (Figure 2). It is reasonable to assume that both compacted buffer and any sedimentary host rock in Canada would have transport capacities that are, within an order of magnitude, similar to those in Opalinus Clay. That being the case, it is apparent from Figure 2 that the advective and diffusive transport of dissolved H_2 cannot transport the corrosion product away from the UFC surface fast enough to avoid the formation of a separate gas phase. The maximum transport capacity for dissolved H_2 is of the order of 10^{-5} $mol_{STP} \cdot m^{-2} \cdot a^{-1}$, which is equivalent to an anaerobic C-steel corrosion rate of only 0.003 $\mu m \cdot a^{-1}$. Therefore, both dissolved and gaseous H_2 are likely to be transported via two-phase flow, for which the capacity in Opalinus Clay is of the order of 10^{-2} $mol_{STP} \cdot m^{-2} \cdot a^{-1}$ or 3 $\mu m \cdot a^{-1}$. At pressures higher than

13 MPa, dilatancy-controlled gas transport is also possible. Whilst this transport mechanism is not believed to cause irreversible damage to the clay structure, there are uncertainties associated with predicting dilatancy-controlled transport and it is advisable at this time to avoid this transport regime. Dilatancy-controlled transport is more likely at corrosion rates of the order of 10 $\mu m \cdot a^{-1}$ or higher.

A number of studies have been carried out on the transport of gas through compacted bentonite and sedimentary deposits (Gallé 1998; Harrington and Horseman 1999, 2003; Hokari et al. 1997; Horseman et al. 1999; Marschall et al. 2005; Nagra 2002, 2004). There is general consensus that the gas pressure builds up until a breakthrough pressure is exceeded, at which time the pressure is released by the formation of a discreet pathway which then re-seals once the pressure drops. The breakthrough pressure is approximately equal to the sum of the hydrostatic and swelling pressures, which for a repository at a depth of 600 m and a bentonite dry density of 1.6 $Mg \cdot m^{-3}$ would be of the order of 6-8 MPa. There is no indication that water is lost from the bentonite upon the release of the gas pressure. If the rate of H_2 generation is sufficiently high, then the gas pathways formed when the gas pressure reaches the breakthrough pressure may be maintained. However, if the rate of H_2 generation is low then these pathways will re-seal until such time that the pressure has reached the breakthrough pressure once again.

Both hydrogen generation and transport are treated in the SCM V1.0. Hydrogen generation is predicted based on the interfacial cathodic processes (Reactions (6) and (7)), the rates of which are determined in the model. Hydrogen transport is modelled as a diffusion process and is assumed to occur both in the saturated phase (dissolved H_2) and in the unsaturated phase (gaseous H_2). The distribution of gas between the dissolved and gaseous forms is determined by Henry's law. When the pressure of H_2 in the unsaturated phase exceeds the breakthrough pressure gas is assumed to be lost from the system and the pressure released.

2.2.5 Treatment of Unsaturated Conditions

One characteristic of a DGR in a sedimentary deposit is that it may take an extended period of time (of the order of tens to hundreds of thousands of years) to fully saturate. As a consequence, there may be an extended period of unsaturated conditions during the anaerobic corrosion phase. The degree of saturation of the buffer affects (i) the rate of transport of species to and away from the UFC (especially of gaseous H_2), (ii) the likelihood of precipitation and film formation, and (iii) the rate of the interfacial electrochemical processes.

Transport of species to and from the UFC surface is assumed to occur by diffusion, at a rate proportional to the effective diffusion coefficient D_{EFF}. For dissolved species, D_{EFF} is simply given by (King et al. 1996)

$$D_{EFF} = \tau_f \varepsilon_e S D_i \qquad (17)$$

where τ_f is the tortuosity factor of the porous layer, ε_e is the effective porosity for mass transport, S is the degree of saturation, and D_i is the diffusion coefficient in bulk solution.

The only gaseous species considered in the SCM V1.0 is H_2, for which the effective diffusivity is given by

$$D_{EFF} = \tau_f \varepsilon_e (1-S)^3 D_g \quad (18)$$

where D_g is the diffusion coefficient of H_2 in the gas phase and it is implicitly assumed that the tortuosity and effective porosity of the gas phase is the same as that in the saturated phase. The dependence of D_{EFF} on the degree of saturation (i.e., $(1-S)^3$) is taken from the dependence of the effective diffusivity of O_2 in unsaturated porous soils (Collin and Rasmuson 1988).

Precipitation of solids is more likely under unsaturated conditions because the loss of water increases the concentration of dissolved solutes. Conversely, as the repository saturates, the concentration of dissolved solutes decreases (assuming no gain or loss of solutes by reaction or transport) and the probability of precipitation diminishes.

It is commonly understood that there exists a threshold relative humidity (RH) below which electrochemical reactions do not occur (Shreir 1976). This threshold RH is typically of the order of 60-70%, although the exact value depends on the nature of the surface contaminants and the porosity of any precipitated corrosion products (King 2006). To account for this phenomenon in the model, the rate constants for the interfacial reactions depend on the surface moisture content h_k as follows:

$$\begin{aligned} k_i &= 0 \qquad \text{for} \qquad h_k \le h_{k,min} \\ k_i &= \frac{h_k - h_{k,min}}{h_{k,max} - h_{k,min}} k_{i,max} \qquad \text{for} \qquad h_{k,min} < h_k < h_{k,max}\ ; \quad i = AF, AB, B, C, D \\ k_i &= k_{i,max} \qquad \text{for} \qquad h_k \ge h_{k,max} \end{aligned} \quad (19)$$

where $k_{i,max}$ is the maximum value of the respective rate constant corresponding to fully saturated conditions, and $h_{k,min}$ and $h_{k,max}$ are the values of h_k between which k_i grows linearly from 0 to its maximum value. The values of $h_{k,min}$ and $h_{k,max}$ are defined by the threshold relative humidity for atmospheric corrosion (60-70% RH) (Shreir 1976).

In the model, the temporal and spatial dependence of the degree of saturation is treated as an external input and is not calculated within the code itself.

2.2.6 Mass Transport

Mass transport is assumed to occur by diffusion only, the hydraulic conductivity of the compacted buffer and host rock being too low to support advective flow. Both the compacted bentonite or bentonite/sand sealing material(s) and the host rock are treated as equivalent porous media. Figure 3 shows the conceptual model used to describe the pore structure of the porous barriers in the SCM (King et al. 1996). Some of the porosity is associated with isolated pores (denoted 1a in Figure 3) and interlammellar spaces between clay particles (1b), both of which are treated as inaccessible to diffusants. Diffusing species, however, can access the through pores (2a) and dead-end or blind porosity (2b). This pore-structure model was developed for compacted bentonite (Oscarson 1994) and, although applied here to all porous media considered in the SCM, the contributions from the individual types of porosity may differ for different media.

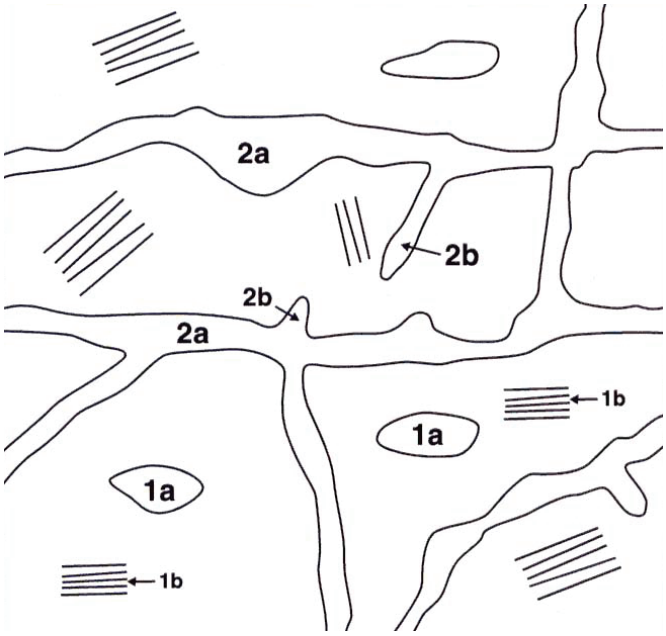

Figure 3: Schematic Illustration of Different Types of Porosity Included in the Conceptual Model for the Equivalent Porous Media in the SCM. The non-accessible porosity is associated with isolated pores (1a) interlamellar regions (1b). The accessible porosity is divided between through pores (2a) and dead-end pores (2b).

Under unsaturated conditions, some of the pore structure will be vapour filled and other parts filled by solution. The distribution of water and vapour between the various types of pore will depend on a number of factors, including their accessibility and size (smaller diameter pores are more likely to be saturated because of capillary effects). In the SCM it is assumed that the distribution of water between the various pores types varies linearly with the degree of saturation (Figure 4).

The mass transport of dissolved and gaseous species is described in the SCM by

$$\frac{\partial(\varepsilon_a S c_i)}{\partial t} = \frac{\partial}{\partial x}\left(\tau_f \varepsilon_e S D_i \frac{\partial c_i}{\partial x}\right) \tag{20}$$

and

$$\frac{\partial((1-S)\varepsilon_a c_g)}{\partial t} = \frac{\partial}{\partial x}\left(\tau_f \varepsilon_e (1-S)^3 D_g \frac{\partial c_g}{\partial x}\right) \tag{21}$$

respectively, where ε_a is the accessible porosity (defined as the sum of the effective porosity for mass transport ε_e and the storage or dead-end porosity ε_s), c_i and c_g are the concentrations of the dissolved and gaseous species, respectively, and all other symbols have been defined above.

Certain species in the model, such as precipitated $Fe(OH)_2$, Fe_3O_4, $FeCO_3$, and $CaCO_3$ and Fe(II) either adsorbed or present in altered clay, are treated as immobile and are assumed not to diffuse.

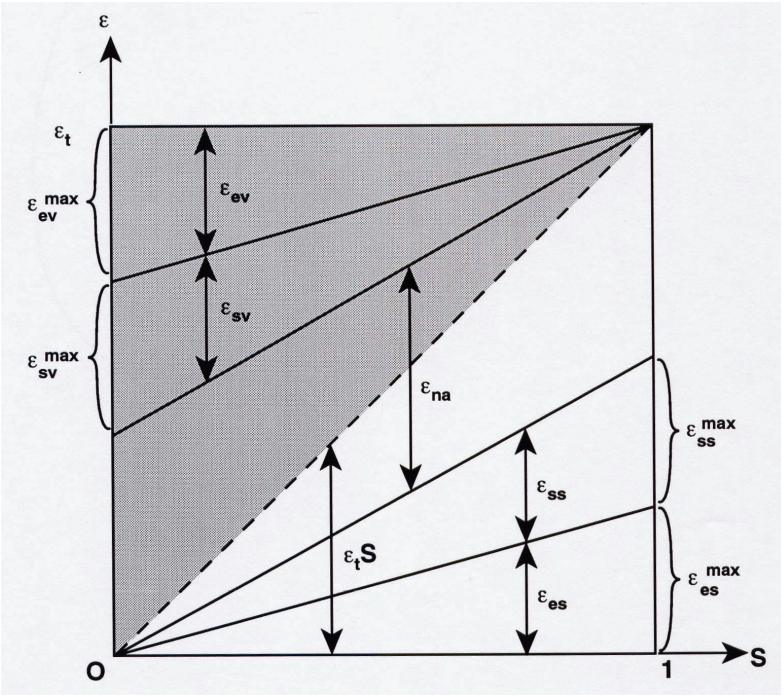

Figure 4: Effect of the Degree of Saturation (S) on the Distribution of Various Types of Porosity in Compacted Buffer (King et al. 1996). The various forms of porosity considered in the conceptual model for compacted buffer are the total porosity ε_t, non-accessible porosity ε_{na}, storage porosity ε_s, and the effective porosity for mass transport ε_e. The additional v and s subscripts on ε_s and ε_e represent the vapour- and solution-phase components, respectively.

2.2.7 Precipitation and Dissolution of Solid Phases

The precipitation and dissolution of solid phases can occur both at the steel/buffer interface and throughout the bentonite sealing materials and host rock. The solid phases included in the SCM V1.0 are $Fe(OH)_2$, Fe_3O_4, $FeCO_3$, and $CaCO_3$. The first three species are corrosion products and, whilst they can theoretically precipitate anywhere within the repository, are most likely to form close to the container surface where the concentrations of dissolved Fe(II) species are highest. The formation and properties of surface films has been described separately above (Section 2.2.2). Calcite ($CaCO_3$) is assumed to be the major source of carbonate within the buffer and host rock.

Ferrous hydroxide ($Fe(OH)_2$) can be formed via the precipitation of dissolved $FeOH^+$ or $FeCl^+$ (Figure 1). Two routes are included for the precipitation of $FeOH^+$ in the model

$$FeOH^+ + OH^- \xrightarrow{k_2} Fe(OH)_2 \qquad (22)$$

and

$$FeOH^+ + H_2O \underset{k_{-11}}{\overset{k_{11}}{\rightleftharpoons}} Fe(OH)_2 + H^+ \qquad (23)$$

The inclusion of two pathways for the precipitation from solution of $FeOH^+$ recognizes the importance of this reaction in the formation of interfacial films. As described in Section 2.2.1.1, there is direct evidence from electrochemical studies for the formation of surface $Fe(OH)_2$ films from an $FeOH^+$ intermediate (Castro and Vilche 1991, 1992; Castro et al. 1991; Odziemkowski et al. 1998; Simpson and Melendres 1996). This process is described in the SCM V1.0 by Reaction (22), the rate of which is assumed to be proportional to the concentration of $FeOH^+$. This reaction is treated as being irreversible since continued dissolution of the steel surface is likely to maintain a high interfacial concentration of $FeOH^+$, thus maintaining a low driving force for the dissolution of $Fe(OH)_2$.

Although it is likely that most of the dissolved $FeOH^+$ will precipitate at the container surface, the possibility of precipitation within the buffer and host rock is included in the model. Because the concentration of dissolved $FeOH^+$ will be lower further away form the container surface, it is possible that precipitated $Fe(OH)_2$ could subsequently dissolve. Therefore, a second, reversible pathway for the precipitation and dissolution of $Fe(OH)_2$ is included in the model (Reaction (23)). Precipitation and dissolution are treated kinetically rather than thermodynamically, with the rate of precipitation assumed to be proportional to the degree of super-saturation of $FeOH^+$ and the rate of dissolution assumed to be proportional to the concentration of $Fe(OH)_2$, the spatial and temporal variation of which is tracked in the model.

Both of these reactions can occur anywhere within the system, although it is considered that Reaction (22) will predominate at the container surface due to the high interfacial concentration of $FeOH^+$.

Ferrous hydroxide may also form via the precipitation of $FeCl^+$

$$FeCl^+ + 2H_2O \underset{k_{-8}}{\overset{k_8}{\rightleftharpoons}} Fe(OH)_2 + 2H^+ + Cl^- \qquad (24)$$

where, again, the precipitation and dissolution processes are treated kinetically. The rate of precipitation of $Fe(OH)_2$ is taken to be proportional to the degree of super-saturation of dissolved $FeCl^+$ and the rate of dissolution to be proportional to the concentration of precipitated $Fe(OH)_2$.

In addition to dissolving to produce either $FeOH^+$ or $FeCl^+$ ions, precipitated $Fe(OH)_2$ may also be converted into one of two further solid phases. As described in Section 2.2.2, $Fe(OH)_2$ is known to convert into Fe_3O_4 via the Schikorr reaction (Odziemkowski et al. 1998). The rate of this process is treated as being proportional to the concentration of $Fe(OH)_2$ (Reaction (9)). Alternatively, $Fe(OH)_2$ may also be converted to $FeCO_3$ (Reaction (10)) at a rate proportional to the concentrations of HCO_3^- and $Fe(OH)_2$.

Once formed, $FeCO_3$ can dissolve to produce soluble ferrous carbonate ions. This process is treated as being reversible, with the precipitation of $Fe(CO_3)_2^{2-}$ serving as an additional pathway for the formation of $FeCO_3$

$$Fe(CO_3)_2^{2-} + H_2O \underset{k_{-5}}{\overset{k_5}{\rightleftharpoons}} FeCO_3 + HCO_3^- + OH^- \qquad (25)$$

The rates of precipitation and dissolution of $FeCO_3$ are taken to be proportional to the degree of super-saturation of $Fe(CO_3)_2^{2-}$ and to the concentration of precipitated $FeCO_3$, respectively.

The source of HCO_3^- is taken to be the dissolution of $CaCO_3$ in the bentonite and/or host rock

$$CaCO_3 + H_2O \xrightarrow{k_{15}} HCO_3^- + Ca^{2+} + OH^- \quad (26)$$

This reaction is treated as being irreversible, which is equivalent to assuming that $FeCO_3$ is more stable than $CaCO_3$. The rate of dissolution is taken to be proportional to the concentration of $CaCO_3$ in the system, with the possibility that the system may become totally depleted of calcite if sufficient siderite ($FeCO_3$) is formed.

2.2.8 Near-field Chemistry

Coupling of the interfacial reactions to the various mass-transport and chemical reactions in the buffer and host rock permit the effect of corrosion on the evolution of the near-field environment to be predicted. In particular, two aspects of the near-field chemistry are predicted within the model, namely: the temporal and spatial distribution of Cl^- ions and the temporal and spatial distribution of HCO_3^-.

Chloride ions do not participate directly in the interfacial corrosion reactions, but are assumed to affect the speciation of dissolved Fe(II) (see below). Evidence available to date indicates that the pore waters in sedimentary deposits in Southern Ontario are highly saline (King 2005b), with Cl^- concentrations that could be in excess of 100 g/L at repository depth. The initial pore-water Cl^- concentration in the compacted bentonite or bentonite/sand mixture may be significantly lower as the buffer may be compacted with potable water with the only source of Cl^- being soluble impurity minerals, such as halite. Over time, the buffer pore water will equilibrate with that in the surrounding host rock and the overall near-field salinity will increase. However, because of the low hydraulic conductivity expected for sedimentary deposits and the correspondingly small volumes of pore water in the host rock, this equilibration process could take some time. Alternatively, the bentonite or bentonite/sand mixture could be compacted with saline solution, in which case the pore-water would be saline from the time of repository closure.

The distribution of carbonate within the near field is predicted in the SCM. The source of carbonate is assumed to be calcite, present both as a mineral impurity in the bentonite and, possibly, in the host rock. Carbonate is important as there is evidence that iron carbonate is the preferred corrosion product in bentonite systems (King 2008a). However, carbonate may be depleted from the near field if extensive $FeCO_3$ formation occurs.

2.2.9 Speciation

Although there are few speciation reactions specifically included in the reaction mechanisms, a number of significant assumptions are made in the model regarding speciation processes in the pore water.

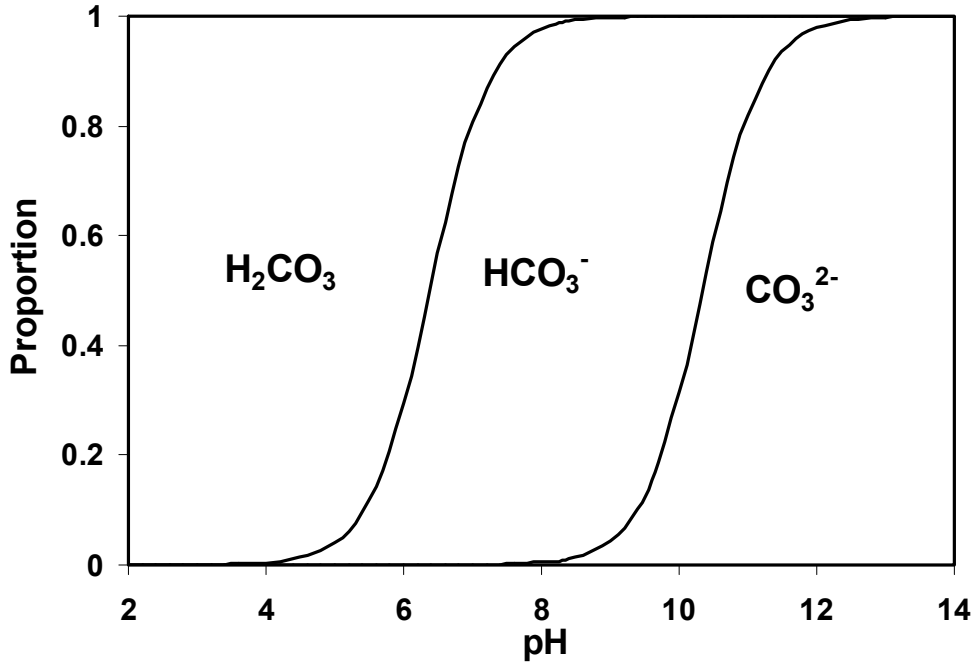

Figure 5: Speciation of Various Carbonate Species as a Function of pH.

The pH of the pore water in the compacted buffer and host rock is assumed to be constant with a value of between pH 7 and pH 9. This value is determined by the buffering by $CaCO_3$, present as an impurity in the bentonite and assumed to be present in the host rock (King 2007, King et al. 2001, Posiva 2006), with the exact value determined by the partial pressure of CO_2 in the pore solution. As a consequence, the predominant carbonate species will be the bicarbonate ion HCO_3^-. Therefore, the carbonate ion CO_3^{2-} is not specifically included in the SCM and all mass balances are performed in terms of HCO_3^-. Furthermore, the concentrations of H^+ and OH^- are not specifically tracked in the model, since it is assumed that there will always be sufficient buffering capacity in the pore solution to maintain a constant pH.

There are a large number of possible dissolved Fe(II) species in the pore water including complexes with chloride, hydroxide, and carbonate ions. If too many species are included in the model then execution of the code slows down. On the other hand, a sufficient number of species need to be included in order to properly represent the pore-water speciation. Figure 6 shows the relative amounts of Fe^{2+}, $FeOH^+$, $Fe(OH)_2$, $Fe(OH)_3^-$, $FeCl^+$, and $FeCl_2$ as a function of pH for Cl^- concentrations of 1 mg/L, 1 g/L, and 100 g/L and for temperatures of 25°C and 100°C. Increasing Cl^- concentration results in a greater fraction of $FeCl^+$ in neutral and moderately alkaline solution, primarily at the expense of Fe^{2+}. With increasing temperature, the Fe(II)-hydroxy species ($Fe(OH)^+$, $Fe(OH)_2$, and $Fe(OH)_3^-$) become more stable at lower pH.

Three different dissolved Fe(II) species are included in the model ($FeCl^+$, $Fe(CO_3)_2^{2-}$, and $FeOH^+$), although the concentrations are not assumed to be in equilibrium. Instead, the concentration of each species is determined by the balance of the rates of the respective formation and consumption processes.

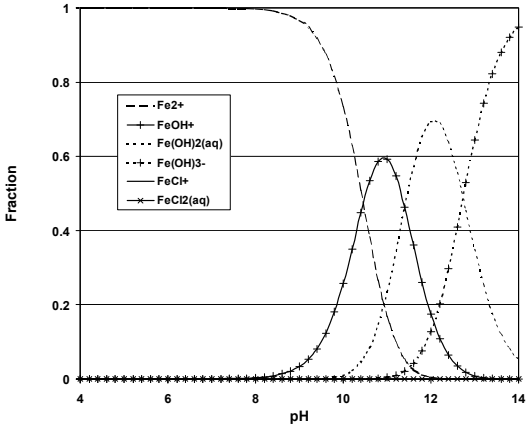

(a) 1 mg/L Cl^-, 25°C

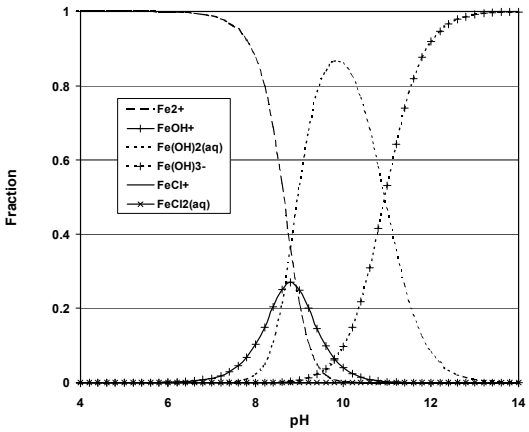

(d) 1 mg/L Cl^-, 100°C

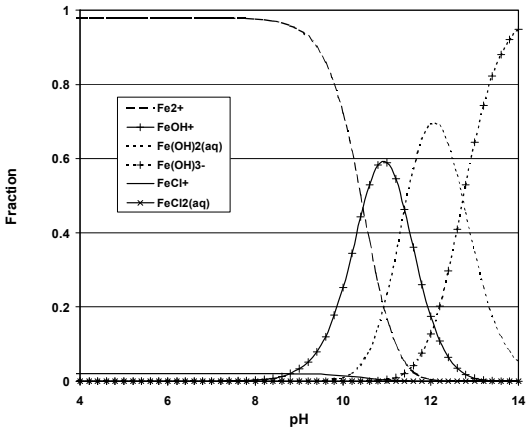

(b) 1 g/L Cl^-, 25°C

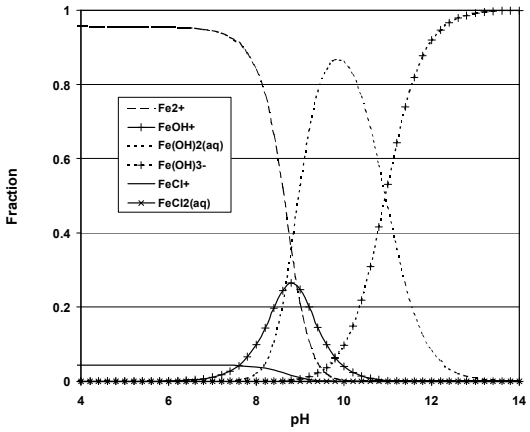

(e) 1 g/L Cl^-, 100°C

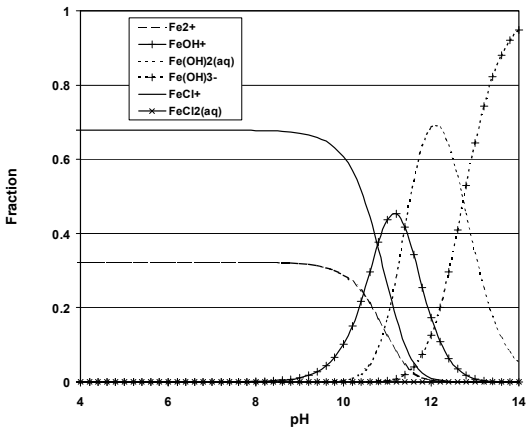

(c) 100 g/L, 25°C

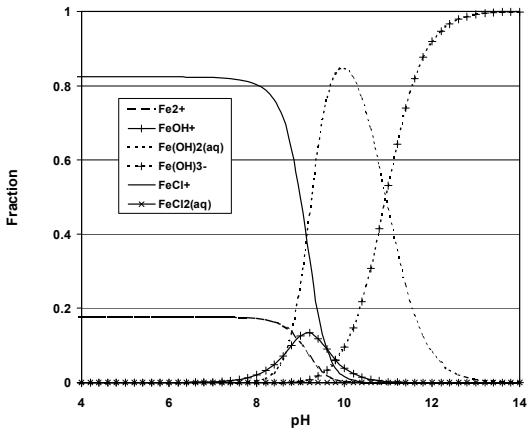

(f) 100 g/L, 100°C

Figure 6: Speciation of Dissolved Ferrous Species as a Function of pH and Chloride Ion Concentration at Temperatures of 25°C and 100°C.

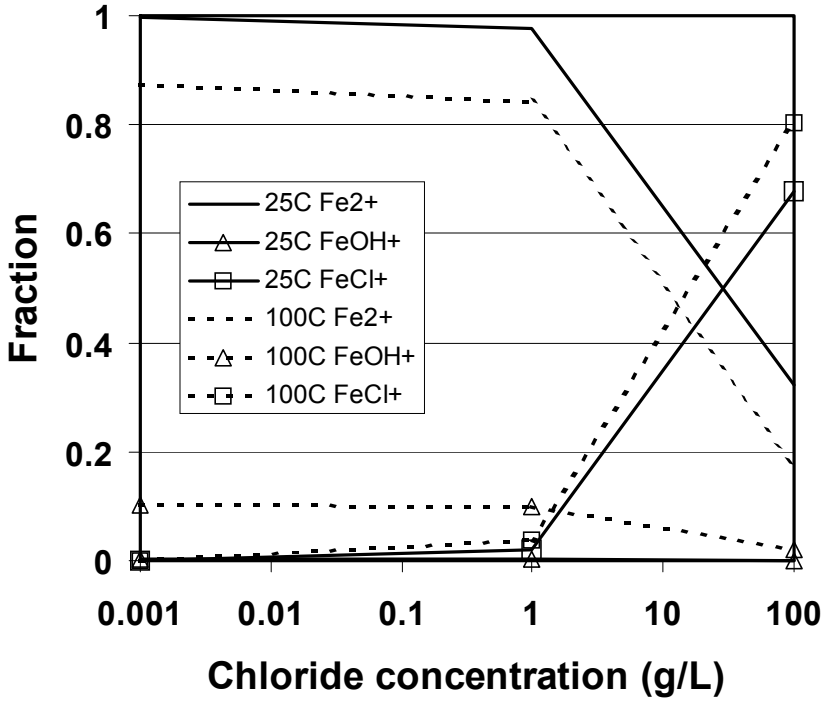

Figure 7: Effect of Chloride Concentration on the Fractions of Fe^{2+}, $FeOH^{+}$, and $FeCl^{+}$ at pH 8 at Temperatures of 25°C and 100°C.

The rationale behind the choice of Fe(II) species to include in the SCM V1.0 is as follows. First, because of the importance of Fe(II) carbonate corrosion products in compacted bentonite (King 2008a), it is necessary to include the Fe(II)-carbonate complex ion $Fe(CO_3)_2^{2-}$. Second, the dissolved species $FeOH^{+}$ is a direct product of the interfacial dissolution reactions (Section 2.2.1.1) and is stable in the range of pore water pH, especially at higher temperature (Figures 6 and 7). Third, of the two species that dominate the speciation at pH 7-9 (i.e., either Fe^{2+} or $FeCl^{+}$), $FeCl^{+}$ was selected for inclusion in the model because of the expected high-salinity pore water in sedimentary host rocks.

2.2.10 Redox Processes

Because the SCM V1.0 is limited to anaerobic conditions, there are no homogeneous redox processes (such as the oxidation of Fe(II) by dissolved O_2 or the reductive dissolution of Fe(III) corrosion products) in the model. Redox process occur during the aerobic and transitional phases in the evolution of the repository environment.

The only processes included in the SCM V1.0 that involve a change in oxidation state are the various interfacial electrochemical reactions and the Schikorr reaction (Equation (9)) involving the conversion of $Fe(OH)_2$ to Fe_3O_4.

2.3 ASSUMPTIONS

Various assumptions are inherent in the SCM V1.0. Table 1 summarizes the various assumptions, together with a discussion of the rationale for each one.

3. MATHEMATICAL MODEL

The mathematical model comprises a series of 1-dimensional mass (and heat)-balance equations, one for each of the 13 species in the model, one for porosity of the precipitated corrosion product, and a heat-conduction equation to enable the spatial and temporal variation in temperature to be predicted. These equations are solved using finite-difference methods subject to various boundary and initial conditions and a spatial grid that represents the geometry of the DGR.

3.1 MASS-BALANCE EQUATIONS

The mass-balance equations for the thirteen chemical species in the model are:

$$\frac{\partial(\varepsilon_a Sc_1)}{\partial t} = \frac{\partial}{\partial x}\left(\tau_f \varepsilon_e S D_1 \frac{\partial c_1}{\partial x}\right) + \varepsilon_a S\left(k_1 c_3 c_6 - k_6 c_1 \rho_d - k_7 c_1 (c_{10}^{max} - c_{10})\rho_d + k_{-7} c_{10} \rho_d - k_8 \max(0, c_1 - c_1^{sat})\right) + k_{-8} c_7 \quad (27a)$$

$$\frac{\partial(\varepsilon_a Sc_2)}{\partial t} = \frac{\partial}{\partial x}\left(\tau_f \varepsilon_e S D_2 \frac{\partial c_2}{\partial x}\right) + \varepsilon_a S\left(-k_{12} c_2 \rho_d - k_{13} c_2 (c_{10}^{max} - c_{10})\rho_d + k_{-13} c_{10} \rho_d - k_5 \max(0, c_2 - c_2^{sat})\right) + k_{-5} c_5 c_9 \quad (27b)$$

$$\frac{\partial(\varepsilon_a Sc_3)}{\partial t} = \frac{\partial}{\partial x}\left(\tau_f \varepsilon_e S D_3 \frac{\partial c_3}{\partial x}\right) + \varepsilon_a S\left(-k_1 c_3 c_6 - k_2 c_3 - k_9 c_3 \rho_d - k_{10} c_3 (c_{10}^{max} - c_{10})\rho_d + k_{-10} c_{10} \rho_d - k_{11} \max(0, c_3 - c_3^{sat})\right) + k_{-11} c_7 \quad (27c)$$

$$\frac{\partial(\varepsilon_a Sc_4)}{\partial t} = \frac{\partial}{\partial x}\left(\tau_f \varepsilon_e S D_4 \frac{\partial c_4}{\partial x}\right) + \varepsilon_a S k_{14} (c_4^{sat} - c_4)(1 - S) c_{13} + k_4 c_7 \quad (27d)$$

$$\frac{\partial(\varepsilon_a Sc_5)}{\partial t} = \frac{\partial}{\partial x}\left(\tau_f \varepsilon_e S D_5 \frac{\partial c_5}{\partial x}\right) + \varepsilon_a S\left(k_5 \max(0, c_2 - c_2^{sat}) + 2k_{12} c_2 \rho_d + 2k_{13} c_2 (c_{10}^{max} - c_{10})\rho_d - 2k_{-13} c_5 c_{10} \rho_d\right) - k_3 c_5 c_7 - k_{-5} c_5 c_9 + k_{15} c_{12} \quad (27e)$$

$$\frac{\partial(\varepsilon_a Sc_6)}{\partial t} = \frac{\partial}{\partial x}\left(\tau_f \varepsilon_e S D_6 \frac{\partial c_6}{\partial x}\right) + \varepsilon_a S\left(-k_1 c_3 c_6 + k_6 c_1 \rho_d + k_7 c_1 (c_{10}^{max} - c_{10})\rho_d - k_{-7} c_{10} \rho_d + k_8 \max(0, c_1 - c_1^{sat})\right) - k_{-8} c_7 \quad (27f)$$

$$\frac{\partial c_7}{\partial t} = \varepsilon_a S\left(k_2 c_3 + k_8 \max(0, c_1 - c_1^{sat}) + k_{11} \max(0, c_3 - c_3^{sat})\right) - k_3 c_5 c_7 - 3k_4 c_7 - k_{-8} c_7 - k_{-11} c_7 \quad (27g)$$

Table 1: List of Assumptions for the SCM V1.0.

Assumption	Comments
The reaction scheme in Figure 1 adequately represents the anaerobic corrosion behaviour of C-steel UFC.	The reaction scheme includes 13 species and incorporates all relevant processes of interest for the anaerobic corrosion of C-steel UFC, including interaction of Fe(II) with bentonite and the generation and release of H_2. The selection of dissolved Fe(II) species is appropriate for the expected repository and host rock environments.
There is no effect of a pre-existing corrosion product film.	An Fe(III)-rich corrosion product film will be formed during the initial aerobic phase, comprising various forms of FeOOH (goethite, lepidocrocite) and green rust. As the repository environment becomes anoxic, it is expected that this film will undergo auto-reductive dissolution, in which reduction of the Fe(III) species in the film is coupled to oxidation of the underlying steel. At the start of the anaerobic period, therefore, there is likely to be a pre-existing film comprising a porous layer of Fe(II) corrosion products (and, possibly, Fe_3O_4). This pre-existing film will have the same effects on the corrosion behaviour as the porous film that develops due to anaerobic corrosion. If the major function of this film is to block surface sites then, as soon as the initial anaerobic corrosion film is deposited, there will be no impact of not considering the pre-existing film. However, if the major effect of the corrosion product film is to restrict mass transport of species towards or away from the surface then not considering the pre-existing film will underestimate the total thickness of the film and, hence, also the corrosion rate.
Mass transport occurs by diffusion only.	Given the low hydraulic conductivity of both the highly compacted buffer surrounding the container and that expected in the host rock (King 2005b), the assumption of diffusive transport only is reasonable.
The repository sealing materials and host rock can be treated as equivalent porous media.	Neither the bentonite-based sealing materials nor the host rock are expected to exhibit discrete fractures. Therefore, their treatment as equivalent porous media is appropriate.
Pore water pH is constant in the range pH 7-9.	This assumption is reasonable provided $CaCO_3$ is present in the buffer and host rock. However, if the carbonate in the system is converted to $FeCO_3$ then the pore-water pH will no longer be buffered. It is unlikely that all calcite in the system will be consumed, although local depletion in the buffer material may be possible.

continued ….

Table 1: List of Assumptions for the SCM V1.0 (continued).

Assumption	Comments
There is a minimum porosity for the precipitated corrosion product layer.	The assumption of a minimum porosity for the corrosion product layer, especially at the interface, is consistent with local acidification inside the pores of the deposit (e.g., due to the hydrolysis of dissolved Fe(II) species). Local acidification, in turn, is consistent with the constant long-term corrosion typically observed experimentally (King 2008a). If there was no minimum interfacial porosity, the corrosion rate would drop to zero as the entire interface became blocked by precipitate, which is inconsistent with experimental evidence.
Maximum surface temperature of container will be 100^{o}C.	Through a combination of UFC spacing and repository design, it is assumed that the maximum container temperature will be 100^{o}C. This temperature limit precludes thermal alteration of bentonite, so that the design properties of the bentonite or bentonite/sand buffer can be assumed.

$$\frac{\partial c_8}{\partial t} = k_4 c_7 \tag{27h}$$

$$\frac{\partial c_9}{\partial t} = \varepsilon_a S k_5 \max(0, c_2 - c_2^{sat}) + k_3 c_5 c_7 - k_{-5} c_5 c_9 \tag{27i}$$

$$\rho_d \frac{\partial c_{10}}{\partial t} = \varepsilon_a S \rho_d \left(k_7 c_1 (c_{10}^{max} - c_{10}) - k_{-7} c_{10} + k_{10} c_3 (c_{10}^{max} - c_{10}) - k_{-10} c_{10} + k_{13} c_2 (c_{10}^{max} - c_{10}) - k_{-13} c_5 c_{10} \right) \tag{27j}$$

$$\rho_d \frac{\partial c_{11}}{\partial t} = \varepsilon_a S \rho_d \left(k_6 c_1 + k_9 c_3 + k_{12} c_2 \right) \tag{27k}$$

$$\frac{\partial c_{12}}{\partial t} = -k_{15} c_{12} \tag{27l}$$

and

$$\frac{\partial ((1-S)\varepsilon_a c_{13})}{\partial t} = \frac{\partial}{\partial x}\left(\tau_f \varepsilon_e (1-S)^3 D_{13} \frac{\partial c_{13}}{\partial x} \right) - \varepsilon_a S k_{14} (c_4^{sat} - c_4)(1-S) c_{13} \tag{27m}$$

where x and t are the spatial and temporal variables, c_i is the concentration of species i, c_i^{sat} is the concentration of a saturated solution in contact with a given solid, the term max(0, $c_i - c_i^{sat}$) ensures that no solid precipitates from an under-saturated solution, c_i^{max} is the maximum concentration of adsorbed species, ρ_d is the dry density of the buffer or host rock, and all other symbols have been previously defined. Table 2 defines the notation for the thirteen species i.

Table 2: Notation and Nature of the Boundary Conditions for the Thirteen Species Included in the SCM V1.0.

	Notation	LHS bc	RHS bc
Aqueous species			
$FeCl^+(aq)$	c_1	ZF	ZC
$Fe(CO_3)_2^{2-}(aq)$	c_2	ZF	ZC
$FeOH^+(aq)$	c_3	E'chem	ZC
$H_2(aq)$	c_4	E'chem	ZF
$HCO_3^-(aq)$	c_5	E'chem	CC
$Cl^-(aq)$	c_6	ZF	CC
Solid or precipitated species			
$Fe(OH)_2(s)$	c_7	-	-
$Fe_3O_4(s)$	c_8	-	-
$FeCO_3(s)$	c_9	-	-
$Fe(II)_{ADS}$	c_{10}	-	-
Fe(clay)	c_{11}	-	-
$CaCO_3(s)$	c_{12}	-	-
			-
Gaseous species			
$H_2(g)$	c_{13}	ZF	ZF

The spatial and time dependence of the porosity is given by

$$\varepsilon_a = \varepsilon_a^{init} - \frac{M_7}{\rho_7}c_7 - \frac{M_8}{\rho_8}c_8 - \frac{M_9}{\rho_9}c_9 \qquad (28)$$

where M_i and ρ_i are the molecular mass and the dry (skeletal) density of the respective solids and ε_a^{init} is the initial accessible porosity of the layer. The initial values of ε_a are defined for the buffer and host rock layers, but not for the corrosion product which is assumed to not initially exist. As the corrosion product layer forms, it is assumed to grow into the adjacent buffer layer producing a layer of mixed bentonite/sand and steel corrosion products, as observed experimentally (King 2008a). A minimum porosity ε_{MIN} is defined for this mixed corrosion product/bentonite layer (typically ε_{MIN} = 0.01) so that the steel surface does not become completely blocked. As the corrosion product continues to form it displaces the buffer from the mixed corrosion product/buffer layer forming a layer of pure corrosion product (King 2008a).

Finally, a heat-conduction equation is included in the model to allow the spatial and temporal variation in temperature to be predicted

$$\rho C\frac{\partial T}{\partial t} = \frac{\partial}{\partial x}\left(K\frac{\partial T}{\partial x}\right) \qquad (29)$$

where T is the absolute temperature and ρ, C, and K are the wet bulk density, the specific heat and the thermal capacity, respectively, of the buffer or host rock.

3.2 MODEL GEOMETRY

In the absence of a specific design for a DGR in Canadian sedimentary host rock, the following discussion is based on a design similar to that proposed by Nagra for a repository Opalinus Clay (Figure 8)

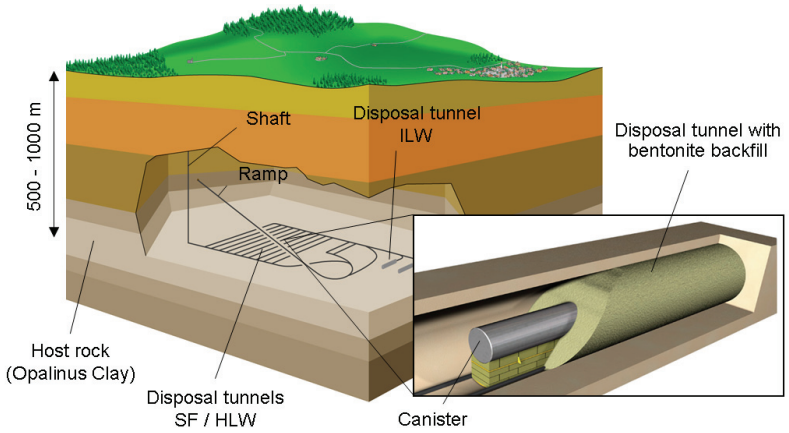

Figure 8: Schematic Illustration of a Deep Geologic Repository in Opalinus Clay in Switzerland (Nagra 2002).

In the Nagra design, the canisters are disposed of within the deposition tunnels which are then backfilled with bentonite clay (Johnson and King 2008). Two different forms of bentonite clay backfill are used; 100% bentonite blocks compacted to a density of 1.6 Mg/m^3 on which the canisters are placed and granular bentonite which is placed around the canisters to fill the deposition tunnel and which, after consolidation, is expected to exhibit an average dry density of 1.45-1.50 Mg/m^3. (The results of thermal analyses suggest that a 70:30 bentonite:sand mixture may be required in a Canadian repository in order to maintain the UFC surface temperature below 100^oC (P. Maak, private communication 2009)). The minimum thickness of bentonite surrounding the canisters is ~70 cm. An excavation-disturbed zone (EDZ) could be created around the tunnel opening during excavation, which may result in a zone with higher hydraulic conductivity (although insufficient to allow advective flow) and/or geochemical changes (e.g., oxidation of pyrite impurities during tunnel operations, resulting in the formation of oxidized S species such as thiosulphate ions). The Opalinus Clay formation is typically of the order of 100 m thick.

A 4-layer geometry is used to represent a Nagra-type repository design for a DGR in Canadian sedimentary host rock (Figure 9). From the UFC surface outwards, these layers are: a layer of variable thickness representing the accumulating corrosion product, a layer of highly compacted bentonite or bentonite/sand mixture, an EDZ layer, and the sedimentary host rock itself. These layers can be further sub-divided if, for example, a more-detailed description of the spatial variation of the degree of saturation is required (King 2008b, King and Kolar 2006).

Each of the buffer and host rock layers is described by the following properties: length or width of the layer; the storage, effective, and non-accessible porosities; the tortuosity factor; dry density; maximum adsorption capacity for Fe(II); the initial concentrations of each of the thirteen species; the initial degree of saturation; and the thermal conductivity and specific heat. Here, the term “initial” refers to the starting time for the code, rather than the time at which the repository is sealed. Therefore, the “initial” degree of saturation and the concentrations of the different species depend on the duration of, and the processes occurring during, the early aerobic and transitional periods.

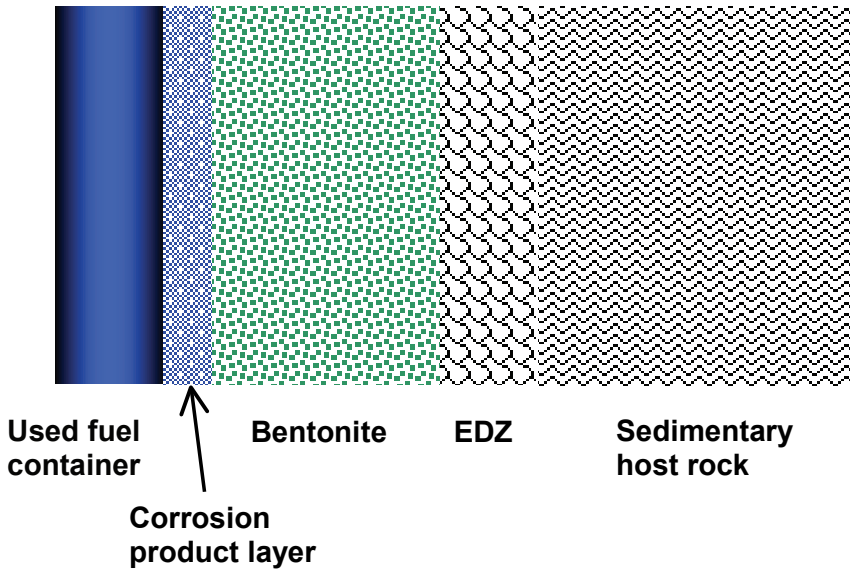

Figure 9: Schematic Illustration of the Geometry of the Various Mass Transport Layers in the SCM V1.0.

There are very few input data requirements required to describe the corrosion product layer. In the SCM V1.0, the corrosion product layer does not exist at the start of the simulation, so that definition of the initial properties is unnecessary. The thickness of this layer is defined by the spatial dependence of the porosity, with the "thickness" being defined by the location at which the porosity decreases significantly. It is assumed that the film does not adsorb Fe(II), comprising as it does a mixture of $Fe(OH)_2$, Fe_3O_4, and $FeCO_3$. The time-dependent degree of saturation of the corrosion product layer is assumed to be the same as that of the adjacent buffer. Furthermore, it is assumed that the relatively thin layer does not affect the thermal profile of the container and surrounding buffer and host rock. Therefore, the only properties that need to be defined are the dry density and the tortuosity factor.

(In subsequent versions of the SCM, it may be possible to include an initial corrosion product layer "thickness." However, because the layer thickness is defined by the spatial (and temporal) variation of the porosity rather than by a formal thickness as such, it would be necessary to define the spatial variation in ε_{CP} at the end of the transitional phase.)

3.3 BOUNDARY CONDITIONS

Mathematical boundary conditions (bc) are required to solve the mass-balance equations (Equations 27(a)-27(m)) for those species that are mobile (i.e., $FeCl^+$, $Fe(CO_3)_2^{2-}$, $FeOH^+$, $H_2(aq)$, HCO_3^-, Cl^-, and $H_2(g)$). For immobile species (i.e., $Fe(OH)_2$, Fe_3O_4, $FeCO_3$, $Fe(II)_{ADS}$, Fe(clay), and $CaCO_3$), the mass-balance equation can be re-formulated to provide the required bc.

3.3.1 Left-hand Boundary

As discussed above, the left-hand boundary of the model represents the UFC surface. For those species that directly participate in interfacial electrochemical reactions on the container surface (i.e., $FeOH^+$, $H_2(aq)$, and HCO_3^-), the corresponding current-potential relationship is used as a type of flux bc.

The anodic dissolution of C-steel is represented in the SCM by the following reaction scheme (Figure 1):

$$Fe + H_2O \underset{k_{AB}}{\overset{k_{AF}}{\rightleftharpoons}} FeOH_{ADS} + H^+ + e^- \qquad (30a)$$

$$FeOH_{ADS} \xrightarrow{k_B} FeOH^+ + e^- \qquad \text{rds} \qquad (30b)$$

At steady-state, the current density (i)-potential (E) relationship for Reaction (30) is given by

$$\frac{i_A}{F} = n_B \frac{k_{AF} k_B}{k_{AB}} \exp\left\{\frac{(1+\alpha_B)F}{RT}\left(E - E^0\right)\right\} \qquad (31)$$

where k_{AF}, k_{AB}, and k_B are the interfacial electrochemical rate constants as defined by Equations (30a) and (30b), n_B and α_B are the number of electrons transferred and the transfer coefficient for the rate-determining step (rds) Reaction (30b), F, R, and T are the Faraday

constant, gas constant, and absolute temperature, respectively, and E^0 is the standard potential. The derivation of Equation (31) is given in Appendix A.

For a value of α_B of 0.5, Equation (31) gives an anodic Tafel slope of 40 mV, consistent with a number of observations reported in the literature (Bockris and Reddy 1970).

Two possible reactions are considered for the accompanying cathodic reaction, the evolution of H_2. The reduction of bicarbonate ions (HCO_3^-) is possible in carbonate-containing environments, via the reaction

$$HCO_3^- + e^- \xrightarrow{k_C} \tfrac{1}{2} H_2 + CO_3^{2-} \tag{32}$$

for which the i-E relationship is

$$\frac{i_C}{F} = -n_C k_C [HCO_3^-]_0 \exp\left\{-\frac{\alpha_C F}{RT}\left(E - E_C^0\right)\right\} \tag{33}$$

where $[HCO_3^-]_0$ is the interfacial concentration of HCO_3^- ions and the other symbols have an analogous meaning to those for Equation (31).

The direct reduction of H_2O is also possible, via

$$H_2O + e^- \xrightarrow{k_D} \tfrac{1}{2} H_2 + OH^- \tag{34}$$

for which the i-E relationship is

$$\frac{i_D}{F} = -n_D k_D \exp\left\{-\frac{\alpha_D F}{RT}\left(E - E_D^0\right)\right\} \tag{35}$$

The reduction of H^+ is another possible cathodic reaction, but is not specifically considered in the SCM as the concentration of H^+ ions is low at the assumed pH of the system of pH 7.5-8. Any H^+ reduction is effectively included in Reaction (34).

At the corrosion potential (E_{CORR}), the sum of the anodic and cathodic currents (and, for a uniformly corroding surface, the current densities) is equal to zero

$$i_A + i_C + i_D = 0 \tag{36}$$

with this equality serving as an additional left-hand bc. At E_{CORR}, the anodic current density equals the corrosion current density i_{CORR}.

The terms i_A, i_C, and i_D can also be related to the interfacial fluxes of the respective reactants or products. Thus,

$$i_A = -n_A F S \tau_f \varepsilon_e D_3 \frac{\partial c_3}{\partial t} \tag{37}$$

$$i_C = -n_C F S \tau_f \varepsilon_e D_5 \frac{\partial c_5}{\partial t} = n_C F S \tau_f \varepsilon_e D_4 \frac{\partial c_4}{\partial t} \quad (38)$$

and

$$i_D = n_D F S \tau_f \varepsilon_e D_4 \frac{\partial c_4}{\partial t} \quad (39)$$

Equations (37)-(39) serve as additional left-hand bc.

For those mobile species that do not participate directly in the interfacial electrochemical reactions, i.e., $FeCl^+$, $Fe(CO_3)_2^{2-}$, Cl^-, and $H_2(g)$, zero-flux conditions are specified for the left-hand boundary (Table 2).

The time dependence of the container surface temperature is used as the left-hand bc for T.

3.3.2 Right-hand Boundary

The right-hand bc are relatively straightforward and are typically defined by either zero-flux, zero-concentration, or constant-concentration conditions (Table 2). Constant concentration bc are used for those species present naturally in the host-rock pore water, such as HCO_3^- and Cl^-. Zero concentration bc are used for those species that are not naturally present in the pore water, such as $FeCl^+$, $Fe(CO_3)_2^{2-}$, and $FeOH^+$. Finally, zero-flux bc are used for $H_2(aq)$ and $H_2(g)$ in order to avoid the loss of hydrogen from the system.

The time dependence of the temperature of the furthest extent of the host rock is used as the right-hand bc for T.

3.4 INITIAL CONDITIONS

The initial conditions are also relatively straightforward. A finite concentration is defined for those species that are present naturally in the pore water or sealing materials, i.e., HCO_3^-, Cl^-, and $CaCO_3$. For all other species, it is assumed that the system is initially free of the corrosion products, i.e., $FeCl^+$, $Fe(CO_3)_2^{2-}$, $FeOH^+$, $H_2(aq)$, $Fe(OH)_2$, Fe_3O_4, $FeCO_3$, $Fe(II)_{ADS}$, Fe(clay), and $H_2(g)$.

The initial condition for T is the spatial temperature distribution at the end of the transitional period.

3.5 NUMERICAL SOLUTION

The numerical finite-difference method used to solve the 1-D reaction-diffusion Equations 27(a)-27(m) subject to the various boundary and initial conditions is described in Appendix B.

4. SUMMARY

The theory underlying the conceptual and mathematical models for the Steel Corrosion Model (SCM) Version 1.0 has been described. The purpose of the model is to predict both the long-term anaerobic corrosion behaviour of a carbon steel used fuel container and also the impacts that this corrosion has on the other repository components. In particular, the effects of alteration of the bentonite clay by Fe(II) corrosion products and of the generation and transport of H_2 gas are of interest. The treatment of the clay alteration reaction is treated quantitatively, so that the extent of such alteration can be predicted. Although the rate of H_2 generation is quantitatively predicted in the model, the consequences for the transport of the gas formed is treated in a conceptual manner, a detailed treatment being outside the scope of the current model.

The model is based on a reaction scheme that encompasses a total of thirteen chemical species, namely: a dissolved ferrous-chloro complex $FeCl^+(aq)$, a dissolved ferrous-carbonate complex ion $Fe(CO_3)_2^{2-}(aq)$, dissolved ferrous-hydroxy ion $FeOH^+(aq)$, dissolved hydrogen $H_2(aq)$, the bicarbonate ion $HCO_3^-(aq)$, the chloride ion $Cl^-(aq)$, solid ferrous hydroxide $Fe(OH)_2(s)$, magnetite $Fe_3O_4(s)$, siderite or iron carbonate $FeCO_3(s)$, adsorbed ferrous species $Fe(II)_{ADS}$, iron-altered clay Fe(clay), calcite $CaCO_3(s)$, and hydrogen gas $H_2(g)$. These species participate in various electrochemical, adsorption/desorption, precipitation and dissolution, clay alteration, mass-transport processes, and partitioning of gases between the aqueous and gaseous phases..

The corrosion behaviour of the used fuel container is described in the model by the time dependence of the corrosion potential E_{CORR} and of the corrosion rate i_{CORR}. The long-term corrosion behaviour is strongly influenced by the formation and properties of corrosion product films. The model allows for the precipitation of $Fe(OH)_2$, Fe_3O_4, and $FeCO_3$ at the container surface and predicts the porosity of the layer as it grows, from which the thickness of the film can be estimated.

Because of the low hydraulic conductivity of sedimentary deposits at repository depth, it is expected that the repository will saturate slowly after closure. The effects of unsaturated buffer on the corrosion of the container are therefore important, and these are also included in the model.

The mathematical model itself is based on a series of 1-D reaction-diffusion equations, which are solved using finite-difference techniques within a spatial grid representing the layout of the repository and surrounding host rock. Inclusion of electrochemical expressions as boundary conditions for the solution of these equations is an important aspect of the model as it allows the development of a mixed-potential model to predict the E_{CORR} and i_{CORR} of the container.

REFERENCES

Albani, O.A., L.M. Gassa, J.O. Zerbino, J.R. Vilche, and A.J. Arvia. 1990. Comparative study of the passivity and the breakdown of passivity of polycrystalline iron in different alkaline solutions. Electrochim. Acta 35, 1437-1444.

Andra. 2005. Dossier 2005 Argile. Andra (Châtenay-Malabry, France, December 2005).

Ashley, G.W. and G.T. Burstein. 1991. Initial stages of the anodic oxidation of iron in chloride solutions. Corrosion 47, 908-916.

Bockris, J.O.'M. and D. Drazic. 1962. The kinetics of deposition and dissolution of iron: effect of alloying impurities. Electrochim. Acta 7, 293-313.

Bockris, J.O.'M. and A.K.N. Reddy. 1970. Modern Electrochemistry. Volume 1. Plenum (New York, NY).

Bockris, J.O.'M, D. Drazic, and A.R. Despic. 1961. The electrode kinetics of the deposition and dissolution of iron. Electrochim. Acta 4, 325-361.

Carlson, L., O. Karnland, S. Olsson, A. Rance, and N. Smart. 2006. Experimental studies on the interactions between anaerobically corroding iron and bentonite. Posiva Working Report 2006-60.

Castro, E.B. and J.R. Vilche. 1991. Electrooxidation/electroreduction processes at composite iron hydroxide layers in carbonate-bicarbonate buffers. J. Appl. Electrochem. 21, 543-551.

Castro, E.B. and J.R. Vilche. 1992. Study of iron electrodissolution in carbonate/bicarbonate solutions by electrochemical impedance spectroscopy. J. Electroanal. Chem. 323, 231-246.

Castro, E.B., S.G. Real, R.H. Milocco, and J.R. Vilche. 1991. The application of electrochemical impedance spectroscopy and identification procedures to the investigation of the dissolution and passivation of iron in carbonate-bicarbonate buffers at 25^{o}C. Electrochim. Acta 36, 117-126.

Collin, M. and A. Rasmuson. 1988. A comparison of gas diffusivity models for unsaturated porous media. Soil Sci. Soc. Am. J. 52, 1559-1565.

Gallé, C. 1998. Migration des gaz et pression de rupture dans une argile compactée destinée à la barrière ouvragée d'un stackage profound. Bulletin Soc. Géol. France, Vol. 169, Part 5, 675–680.

Gierszewski, P., J. Avis, N. Calder, A. D'Andrea, F. Garisto, C. Kitson, T. Melnyk, K. Wei and L. Wojciechowski. 2004. Third Case Study - Postclosure Safety Assessment. Ontario Power Generation, Nuclear Waste Management Division Report 06819-REP-01200-10109-R00. Toronto, Canada.

Harrington, J. F. and S.T. Horseman. 1999. Gas transport properties of clays and mudrocks. In: Muds And Mudstones: Physical And Fluid Flow Properties (eds A.C.Aplin, A.J. Fleet, and J.H.S. Macquaker). Geological Society of London, Special Publication No. 158, 107–124.

Harrington, J.F. and S.T. Horseman. 2003. Gas migration in KBS-3 buffer bentonite. Swedish Nuclear Fuel and Waste Management Company Report, TR-03-02.

Hokari T., M. Okihara, T. Ishii, and H. Ikuse. 1997. Experimental study on scale effects of bentonite/sand mixtures on gas migration. In: Proc. Scientific Basis For Nuclear Waste Management XX, Boston, 2–6 Dec., 1996 (eds W.J. Gray And I.R. Triay), MRS Symposia Proceedings, Vol. 465, Materials Research Society, Warrendale, Pennsylvania, 1019–1026.

Horseman, S. T., J.F. Harrington, and P. Sellin. 1999. Gas migration in clay barriers. Engineering Geology, Vol. 54, 139–149.

Johnson, L.H. and F. King. 2008. The effect of the evolution of environmental conditions on the corrosion evolutionary path in a repository for spent fuel and high-level waste in Opalinus Clay. J. Nucl. Mater. 379, 9-15.

Johnson, L.H., P. Marschall, P. Wersin, and P. Gribi. 2005. HMCBG processes related to the steel components in the KBS-3H disposal concept. Posiva Working Report 2005-09.

King, F. 2005a. Overview of the corrosion behaviour of copper and steel used fuel containers in a deep geologic repository in the sedimentary rock of the Michigan Basin, Ontario. Ontario Power Generation, Nuclear Waste Management Division Report 06819-REP-01300-10101-R00.

King, F. 2005b. Evolution of environmental conditions in a deep geologic repository in the sedimentary rock of the Michigan Basin, Ontario. Ontario Power Generation Nuclear Waste Management Division Report 06819-REP-01300-10102-R00.

King, F. 2006. Review and gap analysis of the corrosion of copper containers under unsaturated conditions. Ontario Power Generation, Nuclear Waste Management Division Report 06819-REP-01300-10124-R00. Toronto, Canada.

King, F. 2007. Overview of a carbon steel container corrosion model for a deep geological repository in sedimentary rock. Nuclear Waste Management Organization Technical Report, NWMO TR-2007-01, Toronto, Ontario.

King, F. 2008a. Corrosion of carbon steel under anaerobic conditions in a repository for SF and HLW in Opalinus Clay. Nagra Technical Report 08-12. Nagra, Wettingen, Switzerland.

King, F. 2008b. Theory manual for the copper corrosion model for uniform corrosion in sedimentary rock CCM-UC.1.1. Nuclear Waste Management Organization Report, NWMO TR-2008-07. Toronto, Canada.

King, F., and M. Kolar. 2000. The copper container corrosion model used in AECL's second case study. Ontario Power Generation Nuclear Waste Management Division Report No: 06819-REP-01200-10041-R00.

King, F. and M. Kolar. 2006. Simulation of the consumption of oxygen in long-term *in situ* experiments and in the third case study repository using the copper corrosion model CCM-UC.1.1. Ontario Power Generation, Nuclear Waste Management Division Report, 06819-REP-01300-10084-R00. Toronto, Canada.

King, F., M. Kolar and D.W. Shoesmith. 1996. Modelling the effects of porous and semi-permeable layers on corrosion processes. In CORROSION/96, NACE International, Houston, TX, paper no. 380.

King, F., L. Ahonen, C. Taxén, U. Vuorinen, and L. Werme. 2001. Copper corrosion under expected conditions in a deep geologic repository. Swedish Nuclear Fuel and Waste Management Company Report, TR-01-23.

Lee, C.T., Z. Qin, M. Odziemkowski, and D.W. Shoesmith. 2006a. The influence of groundwater anions on the impedance behaviour of carbon steel corroding under anoxic conditions. Electrochim. Acta 51, 1558-1568.

Lee, C.T., M.S. Odziemkowski, and D.W. Shoesmith. 2006b. An *in situ* Raman-electrochemical investigation of carbon steel corrosion in Na_2CO_3/$NaHCO_3$, Na_2SO_4, and NaCl solutions. J. Electrochem. Soc. 153, B33-B41.

Maak, P. 1999. The selection of a corrosion-barrier primary material for used-fuel disposal containers. Ontario Power Generation, Nuclear Waste Management Division Report 06819-REP-01200-10020-R00.

MacFarlane, D.R. and S.I. Smedley. 1986. The dissolution mechanism of iron in chloride solutions. J. Electrochem. Soc. 133, 2240-2244.

Marcos, N. 2003. Bentonite-iron interactions in natural occurrences and in laboratory - the effects of the interaction on the properties of bentonite: a literature survey. Posiva Working Report 2003-55.

Marschall, P., S. Horseman, and T. Gimmi. 2005. Characterisation of gas transport properties of the Opalinus Clay, a potential host rock formation for radioactive waste disposal. Oil & Gas Sci. Technol. – Rev IFP 60, 121-139.

Nagra. 2002. Project Opalinus Clay. Safety Report. Nagra Technical Report 02-05.

Nagra. 2004. Effects of post-disposal gas generation in a repository for spent fuel, high-level waste and long-lived intermediate level waste sited in Opalinus Clay. Nagra Technical Report NTB 04-06.

NWMO. 2005. Choosing a way forward. The future management of Canada's used nuclear fuel. Final study. Nuclear Waste Management Organization, Toronto, Ontario.

Odziemkowski, M.S., T.T. Schumacher, R.W. Gilham, and E.J. Reardon. 1998. Mechanism of oxide film formation on iron in simulating groundwater solutions Raman spectroscopic studies. Corros. Sci. 40, 371-389.

Oscarson, D.W. 1994. Surface diffusion: is it an important transport mechanism in compacted clays? Clays Clay Miner. 42, 534-543.

Perronnet, M., M. Jullien, F. Villiéras, J. Raynal, D. Bonnin, and G. Bruno. 2008. Evidence of a critical content in Fe(0) on FoCa7 bentonite reactivity at 80°C. Appl. Clay Sci. 38, 187-202.

Posiva. 2006. Expected evolution of a spent nuclear fuel repository at Olkiluoto, Revised October 2007. Posiva Report 2006-05.

Pourbaix, M. 1974. Atlas of Electrochemical Equilibria in Aqueous Solutions, 2nd. edition. NACE International, Houston, TX.

Russell, S.B. and G.R. Simmons. 2003. Engineered barrier system for a deep geological repository in Canada. In Proc. 10th Int. High-Level Radioactive Waste Management Conf., Las Vegas, NV, March 30-April 2, 2003 (American Nuclear Society, La Grange Park, IL), pp. 563-570.

Ryan, S.R. and F. King. 1994. The adsorption of Cu(II) on sodium bentonite in a synthetic saline groundwater. Atomic Energy of Canada Limited Report, AECL-11062, COG-I-94-125.

Savage, D., C. Watson, S. Benbow, and J. Wilson. 2009. Modelling iron-bentonite interactions. Appl. Clay Sci., in press.

Shreir, L.L. 1976. Corrosion. 2nd edition, Newnes-Butterworths, London.

Simpson, L.J. and C.A. Melendres. 1996. Surface-enhanced Raman spectroelectrochemical studies of corrosion films on iron in aqueous carbonate solution. J. Electrochem. Soc. 143, 2146-2152.

Smart, N.R., D.J. Blackwood, and L.O. Werme. 2001: The anaerobic corrosion of carbon steel and cast iron in artificial groundwaters. SKB Technical Report TR-01-22.

Turnbull, A. and A.T. May. 1987. Steady state electrochemical kinetics of BS 4360 50D structural steel in deaerated 3.5%NaCl solution of varying pH. Brit. Corrosion J. 22, 176-181.

Vela, M.E., J.R. Vilche, and A.J. Arvia. 1986. The dissolution and passivation of polycrystalline iron electrodes in boric acid-borate buffer solutions in the 7.5-9.2 pH range. J. Appl. Electrochem. 16, 490-504.

Wersin, P. and M. Snellman. 2008. Impact of iron on the performance of clay barriers in waste disposal systems. Report on the status of research and development. Posiva Working Report 2008-07.

APPENDIX A: DERIVATION OF ANODIC INTERFACIAL ELECTROCHEMICAL POTENTIAL-CURRENT RELATIONSHIP

The anodic dissolution of C-steel is represented in the SCM by the following reaction scheme (Figure 1):

$$Fe + H_2O \underset{k_{AB}}{\overset{k_{AF}}{\rightleftharpoons}} FeOH_{ADS} + H^+ + e^- \qquad \text{(A-1)}$$

$$FeOH_{ADS} \xrightarrow{k_B} FeOH^+ + e^- \qquad \text{rds} \qquad \text{(A-2)}$$

The mass-balance equation for the intermediate species $FeOH_{ADS}$ is given by

$$\frac{d[FeOH_{ADS}]}{dt} = n_A F A k_{AF} \exp\left\{\frac{\alpha_A F}{RT}\left(E - E_A^0\right)\right\} - n_A F A k_{AB}[FeOH_{ADS}]\exp\left\{-\frac{(1-\alpha_A)F}{RT}\left(E - E_A^0\right)\right\} - n_B F A k_B [FeOH_{ADS}]\exp\left\{\frac{\alpha_B F}{RT}\left(E - E_B^0\right)\right\} \qquad \text{(A-3)}$$

where n, α, and E^0 are the number of electrons transferred, the anodic transfer coefficient, and the standard potential of the two electron-transfer reactions, k_{AF}, k_{AB}, and k_B are the respective electrochemical rate constants, A is the surface area, and F, R, and T are the Faraday constant, gas constant, and absolute temperature, respectively.

At steady state $d[FeOH_{ADS}]/dt = 0$ and

$$[FeOH_{ADS}] = \frac{n_A k_{AF} \exp\left\{\frac{\alpha_A F}{RT}\left(E - E_A^0\right)\right\}}{n_A k_{AB} \exp\left\{-\frac{(1-\alpha_A)F}{RT}\left(E - E_A^0\right)\right\} + n_B k_B \exp\left\{\frac{\alpha_B F}{RT}\left(E - E_B^0\right)\right\}} \qquad \text{(A-4)}$$

The overall anodic current density (i_A) is determined by the rate of the rate-determining step (rds) (Equation (A-2)), which is given by

$$\frac{i_A}{F} = n_B k_B [FeOH_{ADS}]\exp\left\{\frac{\alpha_B F}{RT}\left(E - E_B^0\right)\right\} \qquad \text{(A-5)}$$

Substituting Equation (A-4) into Equation (A-5) gives

$$\frac{i_A}{F} = \frac{n_A n_B k_{AF} k_B \exp\left\{\frac{\alpha_A F}{RT}\left(E - E_A^0\right)\right\}\exp\left\{\frac{\alpha_B F}{RT}\left(E - E_B^0\right)\right\}}{n_A k_{AB} \exp\left\{-\frac{(1-\alpha_A)F}{RT}\left(E - E_A^0\right)\right\} + n_B k_B \exp\left\{\frac{\alpha_B F}{RT}\left(E - E_B^0\right)\right\}} \qquad \text{(A-6)}$$

Since Reaction (A-2) is rate determining

$$n_A k_{AB} \exp\left\{-\frac{(1-\alpha_A)F}{RT}\left(E - E_A^0\right)\right\} >> n_B k_B \exp\left\{\frac{\alpha_B F}{RT}\left(E - E_B^0\right)\right\} \quad \text{(A-7)}$$

Therefore, Equation (A-6) simplifies to

$$\frac{i_A}{F} = n_B \frac{k_{AF} k_B}{k_{AB}} \exp\left\{\frac{F}{RT}\left(E - E_A^0\right)\right\} \exp\left\{\frac{\alpha_B F}{RT}\left(E - E_B^0\right)\right\} \quad \text{(A-8)}$$

If we assume $E_A^0 = E_B^0 = E^0$,

$$\frac{i_A}{F} = n_B \frac{k_{AF} k_B}{k_{AB}} \exp\left\{\frac{(1+\alpha_B)F}{RT}\left(E - E^0\right)\right\} \quad \text{(A-9)}$$

APPENDIX B: NUMERICAL SOLUTION OF REACTION-DIFFUSION EQUATIONS

CONTENTS

APPENDIX B: NUMERICAL SOLUTION OF REACTION-DIFFUSION EQUATIONS

The SCM V1.0 code is based on the reaction-diffusion equations solver TRANSIENT (Kolar 2006). This Appendix is based largely on Section 2 of the theory manual for the current version of TRANSIENT V3.2.

B.1 GENERAL STATEMENT OF THE PROBLEM

The set of reaction-diffusion equations defined above (Equations 27(a)-27(m), (28) and (29)) constitute a set of 15 coupled partial differential equations of the parabolic type which can be written in the form

$$\varepsilon_k(x)\frac{\partial c_k(x,t)}{\partial t} = \frac{\partial}{\partial x}\left(\alpha_k(x,T(x,t))\frac{\partial c_k(x,t)}{\partial x}\right) + R_k(c_i(x,t),x,t) \qquad \text{(B-1)}$$

where x (position) and t (time) are the independent variables, c_i, i=1,...,15 denotes all the dependent variables (the concentrations of the 13 species, the corrosion product film porosity ε_{CP}, and the temperature T), k=1,...,15 represents the equation number, $\varepsilon_k(x)$ is either ε or ρC and is always a piece-wise constant, α_k is the intrinsic diffusivity for the k-th dependent variable, and R_k the reaction terms which are non-linear functions of the concentrations c_i and also of position (via ε, ρ, etc.) and possibly of time). For non-diffusive equations, α_k in Equation (B-1) is identically equal to zero. For equations with piece-wise constant material characteristics ε and τ_f, α_k is also a piece-wise constant with discontinuities only at the inter-media interfaces. These discontinuities have to be accounted for properly (see Equations (B-18) to (B-20) below).

The respective boundary conditions for the diffusive species are of the form

$$\beta_{k,b}\left(\frac{\partial c_i(x_b,t)}{\partial x}, c_i(x_b,t), t\right) = 0 \qquad \text{b = left, right} \qquad \text{(B-2)}$$

Here the explicit time dependence originates from the temperature dependence of the electrochemical rate constants and of the standard potentials. For the non-diffusive species, no special boundary conditions are needed. The “bulk” (homogeneous) non-diffusive equations can be used without any change as the formal boundary conditions for $x = x_{left}, x_{right}$ because in the non-diffusive equations, x is just a parameter. One has to define some “boundary conditions” for all equations, because all have to be treated by the computer code in the same way when solved simultaneously.

B.2 SPATIAL GRID

The spatial grid for the SCM V1.0 has an increasing grid spacing from the left-hand boundary (x = 0) to the right-hand boundary. The grid is finest at the container surface, where the interfacial electrochemical reactions occur and where the concentration gradients are generally the steepest. Inside each medium, the grid spacing increases from left to right according to a geometrical progression. The quotient of this progression is different in each layer.

To build the grid, the grid spacings Δx_λ at the layer interfaces are specified such that $\Delta x_\lambda < \Delta x_{\lambda+1}$. The quotient for the λ-th layer of thickness L_λ is calculated as follows:

$$q_l = \frac{L_l - 2\Delta x_{l-1}}{L_l - 2\Delta x_l} > 1 \qquad \text{(B-3)}$$

Then Δx_λ are adjusted slightly (from left to right) so that there are an exact number of grid intervals, n_λ, within the λ-th layer using the above quotient for the ratio of any two adjacent grid intervals. Using these slightly adjusted values of Δx_λ, the grid points in the λ-th layer are:

$$x_{left,l} + \Delta x_l \frac{q_l^i - 1}{q_l - 1}; \quad i = 0,1,\ldots,n_l \qquad \text{(B-4)}$$

where $x_{left,\lambda}$ is the position of the beginning of the λ-th layer.

B.3 DISCRETIZATION

Both x and t have to be discretized. There are $N = n_1+n_2+\ldots+n_8+1$ grid points x_j given by Equation (B-4), and an *a priori* unspecified number of time instants t_ℓ (ℓ = 0, 1, ...). Values of $c_k(x,t)$ are calculated only at these discrete values of x and t. The concentration and temperature values at these discrete points and times will be referred to as both $c_k(j, \ell)$ and $c_k(x_j,t_\ell)$.

All of the derivatives in Equations (B-1) and (B-2) are replaced by suitable difference formulae. For the time derivative at the j-th grid point, we use the following replacement

$$\frac{\partial c_k(x,t)}{\partial t} \rightarrow \frac{c_k(j,l+1) - c_k(j,l)}{t_{l+1} - t_l} \qquad \text{(B-5)}$$

Here we assume that the solution is already known at t_ℓ and we want to advance it to the next time instant, $t_{\ell+1}$. On the right-hand side (RHS) of Equation (B-1), we can use the usual 3-point central difference formulae for the given type of grid in a differencing scheme of general implicitness (1 - τ), where $0 \le \tau \le 1$; mixing together τ parts of the "old" solution at t_ℓ with (1 - τ) parts of the “new” (to be computed) solution at $t_{\ell+1}$. Let us introduce

$$\bar{c}_i(j) = \tau c_i(j,l) + (1-\tau) c_i(j,l+1), \qquad \text{(B-6)}$$

and substitute this expression for all $c_i(x,t)$ on the RHS of Equation (B-1), and discretize it using suitable difference formulae for the derivatives. Note that $\bar{c}_k(j)$ as defined in Equation (B-6) corresponds to $c_k(x_j,t_\tau)$ at time $t_\tau = t_\ell + \tau(t_{\ell+1} - t_\ell) = \tau t_{\ell+1} + (1 - \tau)t_\ell$, as calculated by linear interpolation between $c_k(j,\ell)$ and $c_k(j,\ell + 1)$. Correspondingly, the last term in Equation (B-1) is replaced by $R_k(\bar{c}_i(j), x_j, t_\tau)$ in this differencing scheme.

Usually, the best choice for τ should be $\tau = 0.5$, corresponding to $t_\tau = (t_\ell + t_{\ell+1})/2$. Note that, in this case only, the error of the difference formula in Equation (B-5) is second order with respect to the time step; otherwise, it is first order. A τ value of 0.5 gives the Crank-Nicholson scheme which, for equidistant grids, is of the second order both in space and time, and for pure diffusion is stable for arbitrary time-step size. It is also stable for large time steps for many types of the reaction term $R_k(c_i(x,t),x,t)$. A τ value of 1 gives the fully explicit scheme, which is stable only for very small time steps, and $\tau = 0$ gives a fully implicit scheme, stable for arbitrary time steps. Thus, $\tau = 0.5$ should give the smallest error due to discretization. However, if there are any problems with convergence, a value of $\tau < 0.5$ should be used.

As α_k = constant in Equation (B-1) in the interior of each medium, we can use the following 3-point central difference formulae at the j-th grid point:

$$\frac{\partial^2 c_i(x,t)}{\partial x^2} \to \frac{2}{\Delta_- + \Delta_+}\left\{\frac{\bar{c}_i(j+1) - \bar{c}_i(j)}{\Delta_+} + \frac{\bar{c}_i(j-1) - \bar{c}_i(j)}{\Delta_-}\right\}, \tag{B-7}$$

$$\frac{\partial c_i(x,t)}{\partial x} \to \frac{1}{\Delta_- + \Delta_+}\left\{\left[\bar{c}_i(j+1) - \bar{c}_i(j)\right]\frac{\Delta_-}{\Delta_+} - \left[\bar{c}_i(j-1) - \bar{c}_i(j)\right]\frac{\Delta_+}{\Delta_-}\right\}. \tag{B-8}$$

where $\Delta_- = x_j - x_{j-1}$ and $\Delta_+ = x_{j+1} - x_j$. These formulae were obtained by requiring that the first three terms of the Taylor series at x_j of the RHS of Equations (B-7) and (B-8) are correct (i.e., equal to the respective LHS). The lowest-order error term of the difference formulae (B-7) and (B-8) are $\bar{c}_i'''$ and $\frac{1}{6}\Delta_+\Delta_-\bar{c}_i'''$, respectively. Here $\bar{c}_i''' = \frac{\partial^3 c_i}{\partial x^3}(x_j, t_r)$. If $\Delta_- = \Delta_+ = h$, Equations (B-7) and (B-8) would be equivalent to the standard equidistant formulae with the error term $O(h^2)$.

Similarly, for j = 0 the following 3-point forward difference formula can be used with Equations (36) to (39)

$$\frac{\partial c_k(x,t)}{\partial x} \to \frac{1}{\Delta_1}\left[-\frac{q+2}{q+1}c_k(0,l+1) + \frac{l+q}{q}c_k(1,l+1) - \frac{1}{q(q+1)}c_k(2,l+1)\right] \tag{B-9}$$

where $\Delta_1 = x_1 - x_0$, $\Delta_2 = x_2 - x_1 = q_1\Delta_1$, and the lowest-order error term is $\frac{1}{6}\Delta_1(\Delta_1 + \Delta_2)c_k'''$. An analogous formula holds for j=N-1, involving q_N and $c_k(j,\ell+1)$ at j=N-3,N-2,N-1.

For interfaces between two media, i.e., if x_j is a grid point at the interface between two media, we have to satisfy the continuity of the diffusive fluxes:

$$\tau_{f-}\varepsilon_- \frac{\partial c_k}{\partial x}(x_{j-}, t) = \tau_{f+}\varepsilon_+ \frac{\partial c_k}{\partial x}(x_{j+}, t), \tag{B-10}$$

Here τ_{f-} and ε_{-} are the values of τ_f and ε to the left of the interface at x_j, and τ_{f+} and ε_{+} those to the right. The usual way of discretizing Equation (B-10) is to replace the one-sided derivatives in the above equations by the following *asymmetric* difference formulae

$$\frac{\partial c}{\partial x}(x_{j^-}, t) \rightarrow \frac{c(j, l+1) - c(j-1, l+1)}{\Delta_-} \tag{B-11}$$

and

$$\frac{\partial c}{\partial x}(x_{j^+}, t) \rightarrow \frac{c(j+1, l+1) - c(j, l+1)}{\Delta_+} \tag{B-12}$$

where c stands for c_k.

However, we prefer to use an alternative (integrational, or mass-balance) approach that proved to give higher precision in cases when a comparison with an analytical solution was possible (Kolar 2006). As explained below, this approach treats all the nodes in the same way, and thus results in discretization that is consistent throughout the whole model. Note that Equation B-7) can also be obtained by integrating $\frac{\partial^2 c}{\partial x^2}$ from $x_j - \frac{\Delta_-}{2}$ to $x_j + \frac{\Delta_+}{2}$, dividing the result by the length of the integration interval, and then applying the following *symmetric* difference formulae

$$\frac{\partial c_k}{\partial x}\left(x_j - \frac{\Delta_-}{2}, t\right) \rightarrow \frac{\bar{c}_k(j) - \bar{c}_j(j-1)}{\Delta_-} \tag{B-13}$$

and

$$\frac{\partial c_k}{\partial x}\left(x_j + \frac{\Delta_+}{2}, t\right) \rightarrow \frac{\bar{c}_k(j+1) - \bar{c}_j(j)}{\Delta_+} \tag{B-14}$$

Let us assume that $c(j,\ell)$ is approximately constant in the vicinity of each grid point, i.e.,

$$\frac{2}{\Delta_+ + \Delta_-} \int_{x_j - \Delta_-/2}^{x_j + \Delta_+/2} c_k(x, t_l)\,dx \rightarrow c_k(j, l) \tag{B-15}$$

and

$$\frac{2}{\Delta_+ + \Delta_-} \int_{x_j - \Delta_-/2}^{x_j + \Delta_+/2} P(c_i(x, t_l), x, t_l)\,dx \rightarrow P(c_i(j, l), x, t_l)\,. \tag{B-16}$$

Then the discretization of Equation (B-1), as described above for the interior grid points in each medium, is equivalent to the following procedure: integrate Equation (B-1) from $x_j - \frac{\Delta_-}{2}$ to $x_j + \frac{\Delta_+}{2}$, to $x_j - \frac{\Delta_-}{2}$ to $x_j + \frac{\Delta_+}{2}$, divide the result by $(\Delta_+ + \Delta_-)/2$ and perform the replacements of Equations (B-5) and (B-13) - (B-16). This amounts to discretizing the integral form of the mass-balance Equation (B-1).

In order to get consistent discretization throughout the whole sample, let us now apply this procedure at all the grid points, including the inter-media boundaries, and also at the outer boundaries 0 and x_{right}. The only modification for the end points results from the fact that the

integration is one-sided, i.e., from 0 to $\frac{\Delta_+}{2}$ for the left outer boundary, and from $x_{right} - \frac{\Delta_-}{2}$ to x_{right} for the right outer boundary.

Let us now perform this integration (or mass-balance) approach to discretization for the grid nodes on an inter-media boundary x_j. Note that for all equations, the reaction terms can be written in the form

$$R_k = \phi_k + \varepsilon_a \psi_k \tag{B-17}$$

where ϕ_k and ψ_k are not explicitly dependent on x. We again assume that $c_k(x,t)$ and $R_D(x,t)$ (and thus also ϕ_k and ψ_k) are constant in the small interval ($x_j - \Delta_-/2$, $x_j + \Delta_+/2$) and equal to their values at x_j, $c_k(x,t) = c_k(x_j,t)$. Integrating the diffusive equations (36a)-(36l) from $x_j - \Delta_-/2$ to $x_j + \Delta_+/2$ gives

$$\left(\varepsilon_{a-}\frac{\Delta_-}{2}+\varepsilon_{a+}\frac{\Delta_+}{2}\right)\frac{\partial c_k(x_j,t)}{\partial t} = D_k\tau_{f+}\varepsilon_{a+}\frac{\partial c_k}{\partial x}\left(x_j+\frac{\Delta_+}{2},t\right)-D_k\tau_{f-}\varepsilon_{e-}\frac{\partial c_k}{\partial x}\left(x_j-\frac{\Delta_-}{2},t\right)$$

$$+\phi_k\frac{\Delta_-+\Delta_+}{2}+\psi_k\left(\varepsilon_{a-}\frac{\Delta_-}{2}+\varepsilon_{a+}\frac{\Delta_+}{2}\right). \tag{B-18}$$

Here, we have used the condition of diffusion flux continuity at the interface (Equation (B-10)). Now dividing both sides of Equation (B-18) by $\frac{1}{2}(\varepsilon_{a-}\Delta_- + \varepsilon_{a+}\Delta_+)$ and using difference formulae Equation (B-5), (B-13) and (B-14) gives

$$\frac{2D_k}{\Delta_-^2(1+q)\varepsilon_{Interface}}\left\{\frac{\tau_{f+}\varepsilon_{e+}}{q}\left[\bar{c}_k(j+1)-\bar{c}_k(j)\right]-\tau_{f-}\varepsilon_{e-}\left[\bar{c}_k(j)-\bar{c}_k(j-1)\right]\right\}$$

$$+\frac{\phi_k+\varepsilon_{Interface}\psi_k}{\varepsilon_{Interface}}-\frac{c_k(j,l+1)-c_k(j,l)}{t_{l+1}-t_l}=0, \tag{B-19}$$

where $\varepsilon_{Interface} = \frac{\varepsilon_{a-}+q\varepsilon_{a+}}{1+q}$ and $q = \frac{\Delta_+}{\Delta_-}$.

Note that the reaction term in Equation (B-19) has exactly the same form as at the interior nodes (Equation (B-17)) except that ε is replaced by $\varepsilon_{Interface}$. The same result is obtained for those of Equations (36) that are non-diffusing (with the diffusion term absent, or B=0). Discretizing these equations in the same way as the other four above, we get

$$\phi_k+\varepsilon_{Interface}\psi_k-\frac{c_k(j,l+1)-c_k(j,l)}{t_{l+1}-t_l}=0. \tag{B-20}$$

Unlike the case of inter-media boundaries, at the outer boundaries the integration approach to discretization does not change the form of the discretized boundary conditions for the non-diffusive equations.

B.4 SOLUTION OF THE RESULTANT ALGEBRAIC EQUATIONS

Upon performing discretization as indicated above, we get a system of n x N equations of the form

$$F_k^{(j)}(c_i(m,l+1), c_i(m,l)) \equiv 0, \tag{B-21a}$$

in n x N unknowns $c_i(m,\ell + 1)$, involving the "old" concentrations, $c_i(m,\ell)$, as known parameters. Here, n=34; k=1,...,n; j = 0,1,..., N - 1; m = 0, 1, 2 for j = 0; m = j - 1, j, j + 1 for $1 \le j \le N - 2$; and m = N - 3, N - 2, N - 1 for j = N -1. For the internal nodes in each medium, the form of $F_k^{(j)}$ is

$$F_k^{(j)} = \sum_{i=0}^{n-1} \mathrm{LIN}(\bar{c}_i(j-1), \bar{c}_i(j), \bar{c}(j+1)) + \frac{P_k(\bar{c}_i(j), x_j, t_\tau)}{\varepsilon_k(x_j)} - \frac{c_k(j,l+1) - c_k(j,l)}{t_{l+1} - t_l}, \tag{B-21b}$$

where LIN( ) represents a linear combination of its arguments. At the inter-media boundaries, $F_k^{(j)}$ is equal to the LHS of Equation (B-19) or (B-20).

This set of non-linear algebraic equations can be solved using Spotnitz's (1994) Newton-Raphson (NR) approach, based on Newman's method (Matlosz and Newman 1987, Newman 1973, Nguyen and White 1987, White 1978) as implemented in the TRANSIENT package (Kolar 206). In this approach, $F_k^{(j)}$ are expanded about a trial point, indicated by $|_0$, using a Taylor series expansion, i.e.,

$$F_k^{(j)} = F_k^{(j)}\big|_0 + \sum_{i=0}^{n-1} \Big\{ A_{k,i}^{(j)} \left[c_i(j-1,l+1) - c_i(j-1,l+1)\big|_0 \right]$$

$$+ B_{k,i}^{(j)} \left[c_i(j,l+1) - c_i(j,l+1)\big|_0 \right] + D_{k,i}^{(j)} \left[c_i(j+1,l+1) - c_i(j+1,l+1)\big|_0 \right] \Big\}, \tag{B-22}$$

where

$$A_{k,i}^{(j)} = \frac{\partial F_k^{(j)}}{\partial c_i(j-1,l+1)}\Big|_0, \tag{B-23}$$

$$B_{k,i}^{(j)} = \frac{\partial F_k^{(j)}}{\partial c_i(j,l+1)}\Big|_0, \tag{B-24}$$

$$D_{k,i}^{(j)} = \frac{\partial F_k^{(j)}}{\partial c_i(j+1,l+1)}\Big|_0. \tag{B-25}$$

Note that $A_{k,i}^{(j)}$ represents an n x n matrix defined for j = 1 to N - 1, $B_{k,i}^{(j)}$ represents an n x n matrix defined for j = 0 to N - 1, and $D_{k,i}^{(j)}$ represents an n x n matrix defined for j = 0 to N - 2.

Because of the difference formulae used at the boundaries, two more matrices must be defined, as follows:

$$X_{k,i} = \frac{\partial F_k^{(j)}}{\partial c_i(2,l+1)}\Big|_0 \qquad \text{for } j=0, \text{and} \tag{B-26}$$

$$Y_{k,i} = \frac{\partial F_k^{(j)}}{\partial c_i(N-3,l+1)}\Big|_0 \qquad \text{for } j=N-1. \tag{B-27}$$

We can write Equation (B-22) in matrix form,

$$\mathbf{J}d\mathbf{c} = -\mathbf{F}\big|_0 \tag{B-28}$$

where

$$J=\begin{bmatrix} \mathbf{B}^{(0)} & \mathbf{D}^{(0)} & \mathbf{X} & & \\ \mathbf{A}^{(1)} & \mathbf{B}^{(1)} & \mathbf{D}^{(1)} & & \\ & \ddots & & & \\ & \mathbf{A}^{(j)} & \mathbf{B}^{(j)} & \mathbf{D}^{(j)} & \\ & & \ddots & & \\ & & \mathbf{Y} & \mathbf{A}^{(N-1)} & \mathbf{B}^{(N-1)} \end{bmatrix}, d\mathbf{c}=\begin{bmatrix} dc^{(0)} \\ dc^{(1)} \\ \vdots \\ dc^{(j)} \\ \vdots \\ dc^{(N-1)} \end{bmatrix}, F\big|_0=\begin{bmatrix} F^{(0)}\big|_0 \\ F^{(1)}\big|_0 \\ \vdots \\ F^{(j)}\big|_0 \\ \vdots \\ F^{(N-1)}\big|_0 \end{bmatrix},$$

$\mathbf{A}^{(j)}$ is the square matrix with elements $A_{k,i}^{(j)}$; k,i = 0,...,n - 1, etc., d**c** is a column vector with elements $dc_i^{(j)}$ = $c_i(j,\ell + 1) - c_i(j,\ell + 1)|_0$; i = 0,...,N -1 , and $\mathbf{F}^{(j)}|_0$ is a column vector with elements $F_k^{(j)}\big|_0$; k = 0,...,n - 1.

J and $\mathbf{F}|_0$ are evaluated at some $\mathbf{c}|_0 = \mathbf{c}^{guess}$, and Equation (B-28) solved for d**c**. If d**c** and $\mathbf{F}|_0$ are less than some specified tolerances, the problem is solved, otherwise $\mathbf{c}^{newguess} = d\mathbf{c} + \mathbf{c}^{oldguess}$ and the process is repeated until convergence is obtained, or signs of divergence or oscillations are detected. In our case, the most suitable initial guess, i.e., the guess for $c_k(j,\ell + 1)$, is obtained by linear extrapolation of $c_k(j,\ell - 1)$ and $c_k(j,\ell)$ to the next time instant $t_{\ell+1}$.

To solve Equation (B-28) for the unknown $dc_i^{(j)}$, we have modified Spotnitz's (1994) algorithm. First an upper-lower decomposition of **J** is performed to get

$$\mathbf{J}d\mathbf{c} = \mathbf{LU}d\mathbf{c} = -\mathbf{F}|_0 \tag{B-29}$$

L and **U** can be written as

$$L=\begin{bmatrix} b^{(0)} & 0 & 0 & & \\ a^{(1)} & b^{(1)} & 0 & & \\ & \cdots & & & \\ & a^{(j)} & b^{(j)} & & \\ & & \cdots & & \\ & & y\ a^{(N-1)} & b^{(N-1)} & \end{bmatrix}, U=\begin{bmatrix} 1 & E^{(0)} & x & & \\ 0 & 1 & E^{(1)} & & \\ & \cdots & & & \\ & & 1 & E^{(j)} & \\ & & \cdots & & \\ & & & 1 & \end{bmatrix}.$$

Let

$$\mathbf{U}d\mathbf{c} = \xi \tag{B-30}$$

so that

$$\mathbf{L}\xi = -\mathbf{F}|_0 \tag{B-31}$$

In the modified algorithm, the Jacobian submatrices (B-23) through (B-27), the elements of the L and U matrices and the components of the ξ vector (using Equation (B-32)) are calculated simultaneously for each grid node, one grid node at a time, starting from j = 0. For all grid nodes j, the same memory is re-used for the Jacobian submatrices and for $a^{(j)}$ and $b^{(j)}$. Similarly, a single n-component vector is used for all $F^{(j)}|_0$. Only $E^{(j)}$ and $\xi^{(j)}$ have to be stored for all j. Finally, the back substitution of Equation (B-30) is done to solve for $dc^{(j)}$.

B.5 ADAPTIVE TIME-STEPPING ALGORITHM

An heuristic adaptive time-stepping algorithm (ATSA) is used. This algorithm is used to select the size of the time step $\Delta t_\ell = t_{\ell+1} - t_\ell$. The above described NR algorithm is then used to advance the solution $c_k(j,\ell)$ at t_ℓ to $c_k(j,\ell + 1)$ at $t_{\ell+1}$. The integration has to be started with a small time step to be able to handle the initial rapid variation in various concentrations and any possible initial singularities. As we are interested in the very long-term behaviour, the time step must eventually be increased as much as possible to complete the integration in a reasonable real time. However, a regular increase (e.g., linear or exponential) of the time step is usually not satisfactory because the rate of change of various concentrations changes with time.

The most often-used, and the simplest, adaptive time-stepping algorithm is based on the maximum[1] change in the value of c_k in one time step $\Delta t_\ell = t_{\ell+1} - t_\ell$

$$\Delta c_{\max}^{(\ell)} = \max_{j,k}\left(w_k \left| c_k(j,\ell+1) - c_k(j,\ell)\right|\right) \tag{B-32}$$

Here w_k are arbitrary weight coefficients that can be introduced for individual species. The algorithm is based on the assumption that $\Delta c_{\max}^{(\ell)}$ is roughly proportional to Δt_ℓ. One requires

[1] Alternatively, a suitable average over all grid node j and dependent variables k can be used instead of the maximum in Equation (B-32). In general, the average is directly proportional to the maximum.

that $\Delta c_{max}^{(\ell)}$ is of the order of a $\Delta c_{max}^{required}$, which is the control quantity of the algorithm and determines the accuracy of the calculation. $\Delta c_{max}^{required}$ is either a constant, a linear or an exponential function of time. If the current value of Δt_ℓ produces $\Delta c_{max}^{(\ell)}$ (as determined by Equation (B-32)), the new value of the time step (to be used for the next integration step starting at $t = t_{\ell+1}$) is simply[2]

$$\Delta t_{\ell+1} = \Delta t_\ell \cdot \frac{\Delta c_{max}^{required}(t_\ell)}{\Delta c_{max}^{(\ell)}}. \qquad \text{(B-33)}$$

The disadvantage of this simple algorithm is that it always tries to maintain $\Delta c_{max}^{(\ell)}$ close to $\Delta c_{max}^{required}$. This may sometimes lead to a very large number of NR iterations, or even failure of the NR procedure (Equations (B-28) to (B-31)) to converge (for some time ranges), because the time step produced by Equation (B-33) is too large. What is needed is an algorithm that will only ensure that $\Delta c_{max}^{(\ell)}$ does not exceed $\Delta c_{max}^{required}$ (strictly or approximately), but that would allow for $\Delta c_{max}^{(\ell)}$ to be much lower than $\Delta c_{max}^{required}$ whenever convergence problems arise.

The dependence of the number of NR iterations needed to achieve convergence in one integration step, n_{inter}, on the value of Δt_ℓ is usually flat and linear (in terms of the smooth line connecting the centres of consecutive steps of this stepwise dependence) for small values of Δt_ℓ, but then it turns up sharply at a certain value of Δt. Beyond this upturn a small increase in Δt_ℓ may lead to a huge increase in n_{iter} and thus to a prohibitive increase in the CPU time. Ideally, we would want to operate just below this sharp upturn. The problem is that the dependence of n_{iter} on Δt_ℓ is not fixed; it usually varies continually with time as the character of c_k changes.

Thus, our heuristic algorithm is based also on n_{iter}. Actually, the "basic" version of the algorithm (corresponding to strict = -1, where strict is a TRANSIENT input control parameter) is based exclusively on n_{iter}. This basic version uses only one control parameter, N_{iter}, which is the required number of NR iterations in one integration step. The algorithm uses as large a time step as possible such that n_{iter} is, *most of the time*, equal to or less than N_{iter}.

The fastest execution in terms of the CPU time should be achieved with the value of N_{iter} corresponding to the onset of that sharp upturn in the dependence of n_{iter} on Δt_ℓ (averaged over time) discussed above. To see which value of N_{iter} results in the shortest CPU time, different values of N_{iter} should be tried, starting from 2, in otherwise identical runs.

This basic version of our ATSA will thus essentially find the largest $\Delta c_{max}^{(\ell)}$ (as a function of time), compatible with a given value of N_{iter}. Often, this may give sufficient accuracy for smaller values of N_{iter}. To check this, the full version of the algorithm is available (invoked with strict $\geq$ 0). The full version links $\Delta t_{\ell+1}$ both to N_{iter} and to $\Delta c_{max}^{required}$; $\Delta t_{\ell+1}$ is essentially the smaller of the value given by Equation (B-33) and the value determined by the basic version of the algorithm as described above. This full version satisfies the requirements for a good ATSA as postulated

[2] If $\Delta c_{max}^{(\ell)}$ exceeds $\Delta c_{max}^{required}$ considerably, one may first want to repeat the current integration step starting at t_ℓ using the reduced time step given by the RHS of Equation (B-33).

above; $\Delta c_{max}^{(\ell)}$ never exceeds $\Delta c_{max}^{required}$ (at least not significantly), but it can be arbitrarily small whenever necessary to prevent convergence problems.

A recommended strategy is to first use the basic version of the algorithm and inspect the resulting $\Delta c_{max}^{(\ell)}$ (shown with monitor=2 and also always output into the diag file), and then to try the full version with successively smaller $\Delta c_{max}^{required}$ until the results (concentrations as function of time) do not change any more. Of course, using very small values of $\Delta c_{max}^{required}$ can increase the execution time considerably.

The current ATSA is based on the lengths of two previous time steps. From their ratio, and from whether the current number of iterations exceeds N_{iter} or not, the ATSA tries to determine a suitable next time step. This extrapolation is always biased towards larger time steps (it tries to push the step upwards whenever possible). If, for the current time instant, TRANSIENT fails to converge, the time step is reduced, and another attempt at convergence is made. Too many recent failures signify that the time step has been increased too fast. Failures are tracked using a variable and, if everything goes well, the contents of this simple history variable should be one most of the time. If the number of failed attempts per time step has grown recently, the value of the history variable stays above 1 for some time. The larger the value, the smaller the upper limit on the maximum allowed time step increase that the algorithm maintains. ATSA usually goes very smoothly, without oscillations in the magnitude of the time step and/or the number of NR iterations, and through any abrupt changes in the evolution of c_k's.

REFERENCES

Kolar, M. 2006. TRANSIENT - A C package for the numerical solution of systems of partial differential equations of parabolic type. http://transient.mkolar.org/.

Matlosz, M. and J. Newman. 1987. Solving 1-D boundary-value problems with BandAid: A functional programming style and a complementary software tool. Computer Chemical Engineering 11, 45-61.

Newman, J. 1973. Electrochemical Systems. Prentice-Hall, Englewood Cliffs, NJ.

Nguyen, T.V. and R.E. White. 1987. A finite difference procedure for solving coupled nonlinear, elliptic partial differential equations. Computer Chemical Engineering 11, 543-546.

Spotnitz, R. 1994. NL3BAND. Technical Software Distributors. Charlotte, NC.

White, R.E. 1978. On Newman's numerical technique for solving boundary value problems. Industrial Engineering Chemical Fundamentals 17, 367-369.